Crash landing of *Vibrio cholerae* by MSHA pili-assisted braking and anchoring in a viscous environment

Wenchao Zhang[1,#], Mei Luo[2,#], Chunying Feng[1], Rachel R. Bennett[3,*], Andrew S. Utada[4,5,*], Zhi Liu[2,*], Kun Zhao[1,*]

[1]*Frontier Science Center for Synthetic Biology and Key Laboratory of Systems Bioengineering (Ministry of Education), School of Chemical Engineering and Technology, Tianjin University, Tianjin, P.R. China*

[2]*Department of Biotechnology, College of Life Science and Technology, Huazhong University of Science and Technology, Wuhan, China*

[3]*School of Mathematics, University of Bristol, Bristol, UK*

[4]*Faculty of Life and Environmental Sciences, University of Tsukuba, Ibaraki, Japan*

[5]*The Microbiology Research Center for Sustainability, University of Tsukuba, Ibaraki, Japan*

[*]Address correspondence to: rachel.bennett@bristol.ac.uk, utada.andrew.gm@u.tsukuba.ac.jp, zhiliu@hust.edu.cn, or kunzhao@tju.edu.cn.

[#] These authors contributed equally.

Abstract

Mannose-sensitive hemagglutinin (MSHA) pili and flagellum are critical for the surface attachment of *Vibrio cholerae*. However, the cell landing mechanism remains largely unknown. Here, combining the cysteine-substitution-based labelling method with single-cell tracking techniques, we quantitatively characterized the landing of *V. cholerae* by directly observing both pili and flagellum of cells in viscous solutions. MSHA pili are evenly distributed along the cell length and can stick to surfaces at any point along the filament. With such properties, MSHA pili are observed to act as a brake and anchor during cell landing which include three phases: running, lingering, and attaching. Resistive-force-theory based models are proposed to describe near-surface motion. Importantly, the role of MSHA pili during cell landing is more apparent in viscous solutions. Our work provides a detailed picture of the landing dynamics of *V. cholerae* under viscous conditions, which can provide insights into ways to better control *V. cholerae* infections.

Introduction

Vibrio cholerae, a human pathogen that causes the debilitating disease cholera, is a natural inhabitant of aquatic ecosystems (*Almagromoreno et al., 2015; Kaper J B, 1995*). They can form biofilms on both biotic and abiotic surfaces, which increases their infectivity and environmental survival (*Donlan et al., 2002; Silva et al., 2016; Teschler et al., 2015; Yildiz et al., 2009*).

Bacterial appendages have been shown to play important roles in regulating bacterial activities especially biofilm formation during microbe-host interactions. The flagellum is required for biofilm formation in a variety of bacteria species, such as *E. coli* (*Pratt et al., 1998*), *P. aeruginosa* (*O'Toole et al., 1998*), and *V. cholerae* (*Guttenplan et al., 2013; Watnick et al., 1999*). Mutants lacking flagella in both *E. coli* and *Vibrio vulnificus* have been observed to be defective for attachment (*Friedlander et al., 2013; Lee et al., 2004*). Type IV pili (TFP) are another type of filamentous appendages commonly found on many bacteria and archaea, which have diverse functions such as cellular twitching motility, biofilm formation, horizontal gene transfer, and host colonization (*Piepenbrink et al., 2016*). *P. aeruginosa* display two types of TFP-driven twitching motility (*Gibiansky et al., 2010*). *Neisseria gonorrhoeae* have shown a TFP-dependent attachment, leading to the formation of microcolonies on host cell surfaces (*Higashi et al., 2007*). In contrast, although *V. cholerae* biosynthesize three types of TFP that are expressed under different scenarios, they have not been observed to twitch on surfaces. These three pili are: chitin-regulated competence pili (ChiRP; formerly termed PilA), toxin co-regulated pili (TCP), and mannose-sensitive hemagglutinin type IV pili (MSHA) (*Meibom et al., 2004; Reguera et al., 2005; Yildiz et al., 2009*). ChiRP pili were observed to be able to grasp extracellular DNA and transport it back to the cell surface via pili retraction (*Ellison et al., 2018*). TCP pili are important for host colonization and pathogenesis (*Kirn et al., 2000; Thelin et al., 1996*). In contrast to these two types, MSHA pili are known to be important for surface attachment of *V. cholerae* (*Utada et al., 2014; Watnick et al., 1999*).

Motility has been shown to be a crucial element for *V. cholerae* colonization of the epithelium, leading to successful infection of the human host (*Krukonis et al., 2003; Tsou et al., 2008*). Two types of near-surface motility, roaming and orbiting, were observed in *V. cholera* (*Utada et al., 2014*). It has been further suggested that *V. cholerae* synergistically employ the use of their flagella and MSHA pili to enable a hybrid surface motility that facilitates surface selection and attachment (*Utada et al., 2014*). However, there is a lack of direct observational evidence of the appendages in question. More importantly, the environmental niches *V. cholerae* encounter in their life cycle typically include highly viscous mucus (*Almagromoreno et al., 2015*). The mucus layer of animal intestines is estimated to have a wide range of viscosities, varying anywhere from the viscosity of water (~1 cP) to 1000-fold higher (1000 cP) (*Lai et al., 2009*). How cells land on surfaces in highly viscous environments is still not clear. To answer these questions, direct live-cell visualization of the pili and flagellum in real-time in viscous conditions is needed.

Recently, there have been significant advances in techniques for directly observing cell appendages (*Blair et al., 2008; Ellison et al., 2019; Ellison et al., 2018; Ellison et al., 2017; Nakane et al., 2017; Renault et al., 2017; Skerker et al., 2001; Talà et al., 2019*). Among them, the cysteine substitution-based labelling method is specific and has been successfully applied to visualize tight adherence (TAD) pili of *C. crescentus* and type IV pili of *V. cholera* (*Ellison et al., 2019*).

In this paper, by combining a cysteine substitution-based labelling method with single-cell tracking, we directly observed the individual pili and flagellum of landing cells in viscous media and revealed the dynamic landing sequence of *V. cholerae* as it makes initial surface attachment. Resistive-force-theory (RFT) based hydrodynamic models are developed to aid in describing bacterial behavior. The role of MSHA pili during cell landing in highly viscous environment is demonstrated. Our work provides a

detailed picture of the landing dynamics of *V. cholerae* under viscous conditions, during which, the synergistic functions of MSHA pili and flagellum are elucidated.

Results

MSHA pili are evenly distributed along cell length with a constant length density

To visualize the MSHA pili, we constructed a mutant (MshAT70C) by cysteine substitution, which can subsequently be labeled with highly-specific maleimide dyes (*Figure 1*a and *Figure 1-Figure supplement 1*), following the protocol in Ellison *et al*. (*Ellison et al., 2019; Ellison et al., 2017*). The results of Hemagglutination assays confirm that the point mutation in MSHA of the mutant does not affect MSHA pilus function (*Figure 1-Figure supplement 2*). To observe the distribution of MSHA pili on the cell surface, we simultaneously stained the plasma membrane with FM4-64 in Figure 1a.

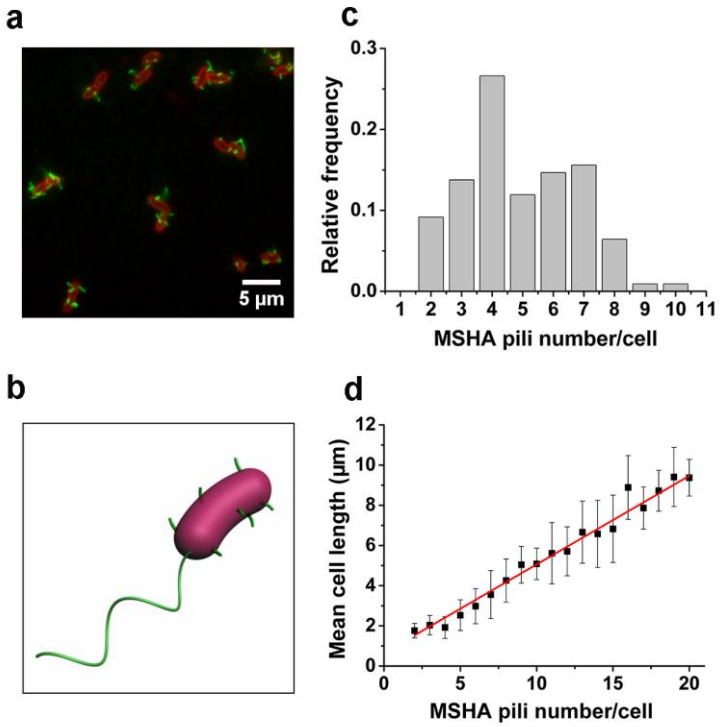

Figure 1. MSHA pili are evenly distributed along cell length with a constant length density. (a) Examples of labeled MSHA pili observed on cell bodies. Green fluorescence showing the AF488-mal labeled MSHA pili, red fluorescence showing the FM4-64 labeled plasma membrane. (b) A 3D view of

a typical *V. cholerae* cell showing the whole body distribution of MSHA pili; this cell has 6 pili. (c) Distribution of pili number per cell cultivated in LB medium. $N_{cell} = 110$. (d) The MSHA pili number per cell is linearly correlated with the cell length. Cells with longer length were obtained by 30~50 min treatment using 10 μg/mL cephalexin. $N_{cell} = 368$.

Figure 1-Figure supplement 1. Labeling of *V. cholerae* MSHA pilus protein MshA with AF488-mal.

Figure 1-Figure supplement 2. Hemagglutination assays.

Figure 1-Figure supplement 3. MSHA pili labeling during cell growth.

We visualized the positions of the different pili as the cell body rotates by recording high speed movies during surface landing. Figure 1b shows a three-dimensional model of a single cell reconstructed from the movies. The results show evenly distributed MSHA pili along the cell length, indicating absence of preferred pili localization on the cell body. Quantitatively, we find that the majority of cells have approximately 3~7 MSHA pili, with 4 MSHA pili per cell being observed most frequently, as shown in Figure 1c. These results are in agreement with recent reports (*Floyd et al., 2020*). Under our conditions, we observed MSHA pili growth (*Figure 1-Figure supplement 3*a and b) but no retraction.

The number of MSHA pili appears to be positively correlated with cell length since it increases as the cell grows (*Figure 1-Figure supplement 3*c). Statistically, the number of MSHA pili shows a linear relationship with cell length (Figure 1d), indicating that the length density of MSHA pili is roughly constant for *V. cholerae*.

MSHA pili mediate *V. cholerae* landing by acting as a brake and anchor

The MSHA pili, which are uniformly distributed across the cell surface, play a crucial role in surface attachment of *V. cholerae* through pili-surface interactions (*Utada et al., 2014*). To elucidate the role of MSHA pili in the landing dynamics under viscous conditions, we directly visualize the fluorescently

117 labeled MSHA pili on *V. cholerae* swimming in a highly viscous medium consisting of 2% LB and 1%
118 MC (LB+MC).

119 Consistent with previous reports in normal aqueous solutions (*Utada et al., 2014*), the WT strain in
120 LB+MC also exhibits orbiting behavior, characterized by multi-pass circular trajectories, and roaming
121 behavior, characterized by highly exploratory, diffusive, trajectories. Typical roaming and orbiting
122 trajectories in LB+MC are shown in Figure 2 (see more examples in *Figure 2-Figure supplement 1*).
123 The roaming cell traces out a path that is linear trajectory over short distances, with a radius of gyration
124 R_g =19.5 μm, and an average speed of 1.7 μm/s (see *Figure 2*a, b, Movie S1). In contrast, the orbiting
125 cell trajectory is much more circular with an average R_g=1.6 μm and an average speed of 1.1 μm/s (see
126 *Figure 2*c, d, Movie S2). A 3D plot of speed plotted along the trajectory in both examples show that
127 both phenotypes make momentary pauses, where their speed slows down; this can be seen clearly in
128 Figure 2b, where the cell motion near a surface displays a characteristic alternation between moving and
129 stopping (*Figure 2*b and 2d).

130 Such pauses are suggested to be caused by MSHA pili-surface interactions (*Utada et al., 2014*).
131 However, by recording fluorescence movie sequences, we directly visualized the process, thereby
132 providing direct evidence that the pauses are due to transient contact between MSHA pili and surface.
133 We show a transient pili-surface contact during orbiting in Figure 2e. In a sequence of frames, we see a
134 transiently attached pilus become stretched due to cell motion away from the point of attachment.
135 Subsequently, this pilus detaches from the surface as the cell continues to move, as indicated with the
136 white arrowheads in Figure 2e (for more details, see Movie S2). These results indicate that the MSHA
137 pili can work as a brake to abruptly slow-down cell motion by transiently attaching to the surface. This
138 is further confirmed by the observation that during the course of surface motion, different MSHA pili
139 attach and detach, switching dynamically as the cell uses these as transient attachment points (*Figure 2-*

Figure supplement 2 and Movie S3). Such a switching of the specific MSHA pili that are engaging the surface is caused by the rotation of cell body, which is required to balance the torque for flagellar rotation when cells swim. Thus, as the cell body rotates due to the rotation of the flagellar motor, different MSHA pili distributed on the cell body take turns approaching and receding from the surface. The switching of attached MSHA pili not only continues to slow-down cell motion but also changes the direction of motion. Taken together, this indicates that the pili distribution on the cell body may also affect cell-surface motion.

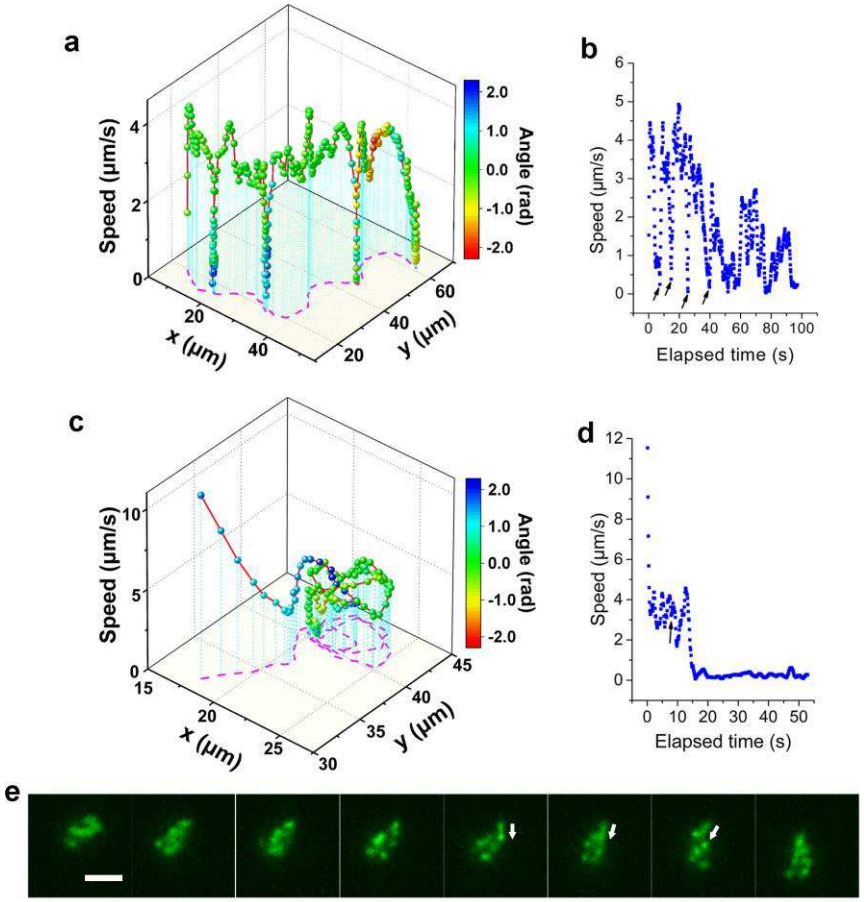

Figure 2. Analysis of roaming and orbiting, using cells of MSHA labelled MshAT70C. The 3D plot and speed changes over time of representative (a-b) roaming and (c-d) orbiting cells, respectively. The magenta dashed lines in panel (a) and (c) are the trajectories of cells and the color maps mean the angle

151 changes over time. The arrows in panel (b) represent temporary attachment between MSHA pili and
152 surface, where the speeds are close to 0. (e) Time-sequence snapshots of the orbiting cell in panel (c-d)
153 at 130 ms intervals. The arrowheads show the stretched pilus, which corresponds to the black arrow in
154 panel (d), indicating temporary attachment of pilus on the surface. Scale bar, 2 μm.

155 **Figure 2-Figure supplement 1.** Quantitative analysis of roaming and orbiting by MSHA labelled
156 MshAT70C in 2% LB with 1% MC.

157 **Figure 2-Figure supplement 2.** Switch of temporary attached pili.

158

159 When the adhesion between MSHA pili and surface is sufficiently strong, the attachment point can act
160 as an anchor point. We demonstrate this by showing the deflection of the trajectory of a swimming cell
161 by the attachment of a, single, anchoring MSHA pilus; here, linear motion is bent into circular motion
162 that is centered around the attachment point (see Movie S4). We estimate the centripetal force for this
163 motion to be on the order of 10^{-21} N, which is much smaller than the pN forces that pili can sustain
164 (*Floyd et al., 2020; Maier et al., 2002*). The anchoring of MSHA pilus eventually leads to the
165 irreversible attachment of the cell.

166 **The landing sequence of *V. cholerae* includes three phases**

167 To further clarify the landing process, we labelled both flagellum and pili simultaneously using
168 MshAT70CFlaAA106CS107C mutant. Figure 3 shows an example of the complete landing process of
169 an orbiting cell. Based on the pattern of motion displayed by the cell (*Figure 3*a and Movie S5), we
170 divide the landing process into three phases: running, lingering, and attaching. In the running phase (0-
171 3.77 s), cells will swim and can perform roaming or orbiting. We note that misalignments between the
172 flagellum and cell body axis tend to change the motion direction of the cell (*Figure 3*a, b). In the
173 lingering phase (3.77-4.68 s), the cells demonstrate one of two states: a paused state or a tethered state,

where the cell can move under the constraint of tethering pilus (see *Figure 3*a for the tethered state). At 3.77 s, one pilus attaches to the surface and acts as an anchor point to prevent the cell from moving away. Finally, in the attaching phase (≥ 4.68 s), cells remain on the surface motionless during the observation period most likely since they have effected irreversible attachment. Upon irreversible cell attachment, some of the free MSHA pili become attached to the surface firmly while others demonstrate fluctuations punctuated with intermittent attachment to the surface (Movie S6). We can measure the persistence length of MSHA pili from the thermal fluctuations of broken MSHA pili (*Figure 3-Figure supplement 1* and Movie S7) to be ~0.15 μm; this value is much smaller than 5 μm persistence length of *P. aeruginosa* TFP (*Skerker et al., 2001*).

During cell landing, transitions between the running and lingering phase, as well as between the two states of lingering phase are observed. The measured conditional probabilities q_{ij} that a cell transitions from state i to j show that the running phase has a relatively lower q_{rt} to the tethered state (~22%) but a higher q_{rp} to the paused state (~78%). Similarly, the paused state has a higher q_{pr} than q_{pt}. In contrast, the tethered state shows similar q_{tr} and q_{tp}, which are 45% and 55%, respectively (*Figure 3*c).

The single-cell dynamics in each specific phase/state is also characterized quantitatively. In the running phase of *V. cholerae*, we found that the period for body rotation is generally distributed between 0.25-2 s and is centered at ~0.7 s (the rotation rate was ~1.5 Hz) in LB+MC (*Figure 4*a). We measure the swimming speed, v, and the cell-body rotation rate, ω_c, for each cell, and plot v as a function of ω_c (see *Figure 4*b). By fitting the data, we found that v linearly increases with ω_c with a slope of $|v/\omega_c| =$ 0.39 μm/radian.

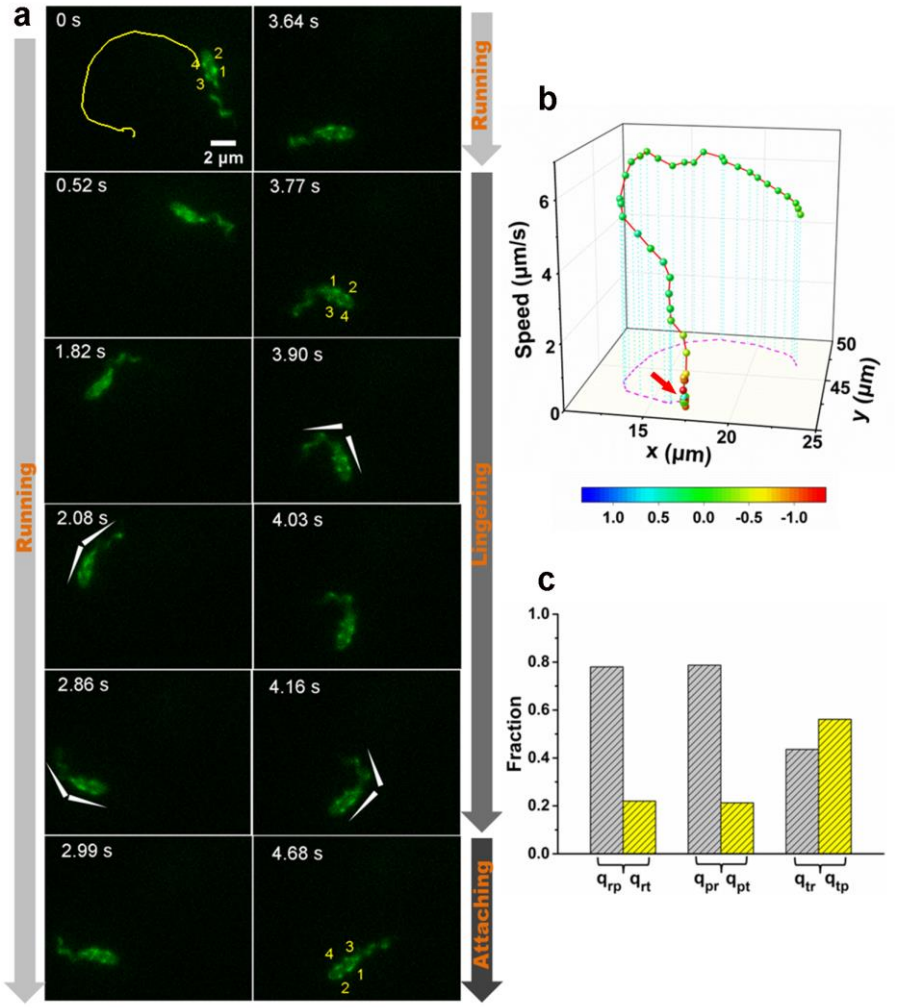

Figure 3. An example of a typical landing sequence of a *V. cholerae* cell with MSHA pili and flagella both labelled (MshAT70CFlaAA106CS107C). (a) Representative image sequences showing the behavior of MSHA pili and flagella. For easy identification, four pili of the example cell in Figure 3a were numbered from 1 to 4, which revolve around the major axis of the cell periodically as the cell swims. The white arrowheads indicated the orientation of cell body and flagellum. (b) A 3D plot of speed and angle changes of the representative cell in panel (a) over its trajectory. The red arrow in panel (b) represents the position, where the pili touch surface, causing a deflection. (c) The conditional probabilities q_{ij} that the bacterium transitions from state i to j. The number of transition events used for estimating these conditional probabilities is 666. r: running state, t: tethered state, p: paused state.

Figure 3-Figure supplement 1. Motion of the broken MSHA pilus.

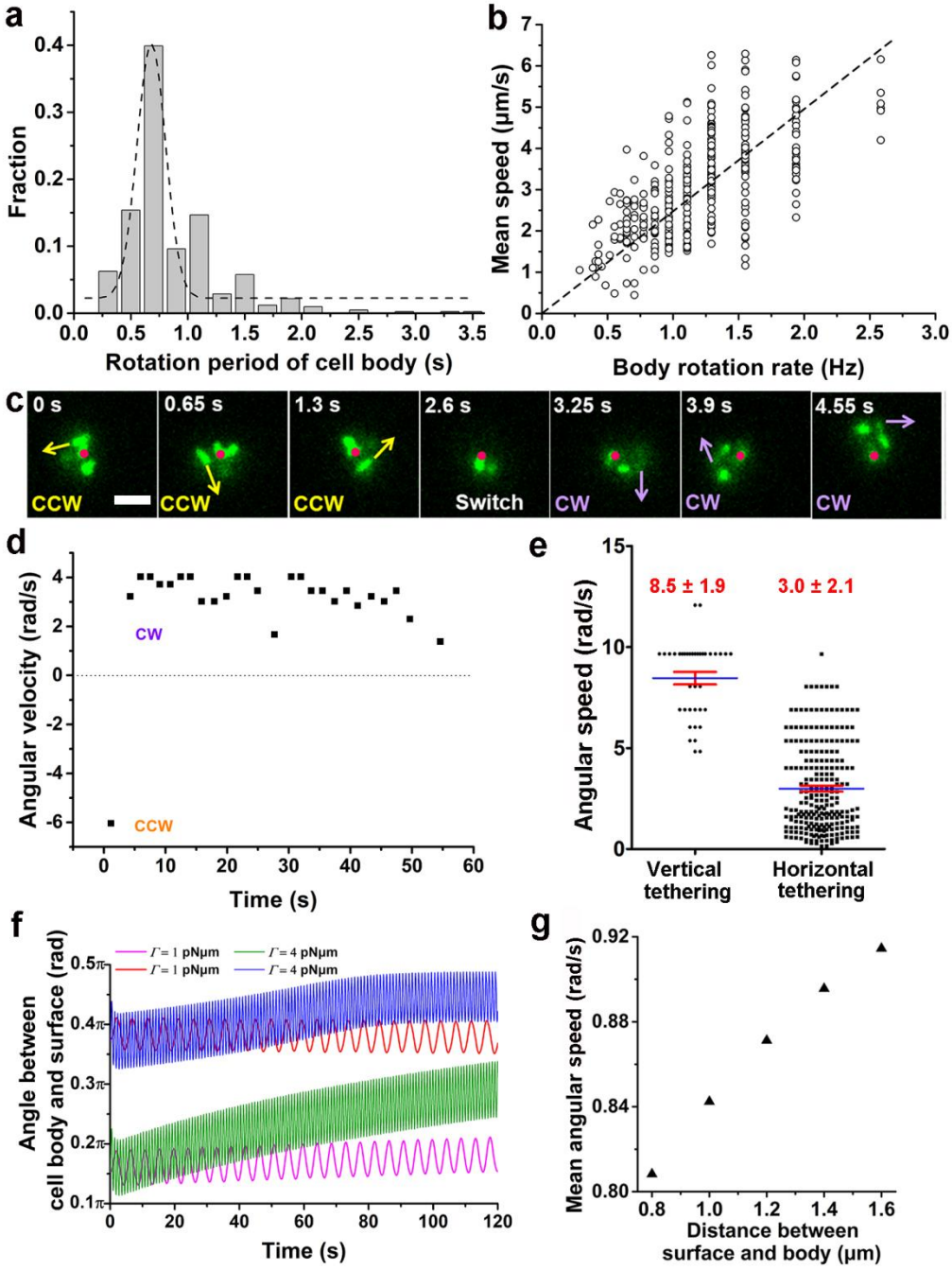

Figure 4. Characterization and RFT-based modeling of running and tethered cells. (a) Distribution of the rotation period of cell body. The dashed line represents Gaussian fitting. A total of 416 rotation events from 54 cells were used for statistical analysis. (b) Measured relation between the rotation rate of

cell body and the mean swimming speed of cell. The dotted line represents linear fitting result. N_{cell} = 47. (c) An example of a typical tethered motion, showing cell performing a circular motion around a center point (the red dot) with the direction of motion (noted by arrows) switched from CCW to CW. Scale bar, 2 μm. (d) The angular velocity of the tethered cell in panel (c) over a short duration showing a pair of CW (positive angular velocity) and CCW(negative angular velocity) intervals; (e) Distribution of angular speed of circular motion for horizontal (241 intervals from 25 cells) and vertical (38 intervals from 5 cells) tethered cells. (f) Hydrodynamic model predicts that motor torque affects preferred tilt angle. The angle that the cell makes with the surface is shown for two choices of motor torque, Γ=4 pN·μm (green, blue) and Γ=1 pN·μm (magenta, red), and two choices of initial tilt angle, θ=0.5 rad (magenta, green) and θ=1.2 rad (red, blue). For Γ=4 pN·μm the cell moves towards a tilt angle close to vertical, independent of initial condition, whereas for Γ=1 pN·μm the tilt angle stays close to the initial condition. The distance between the surface and the constrained cell pole used here is 1 μm. (g) The angular speed about the direction normal to the surface decreases as the closest distance between the cell body and the surface decreases. Angular speeds are shown for motor torque Γ=1 pN·μm with initial tilt angle 0.6 rad.

Figure 4-Figure supplement 1. Examples show positions of two poles and centroid of tethered motility.

By contrast, a cell in the tethered state typically performs a circular motion around the attachment point (red dots in *Figure 4*c). The direction of the circular motion is also dynamic and can switch from counter-clockwise (CCW) to clockwise (CW) presumably due to a switch in the rotation direction of the flagellar motor (see 2.6 s, *Figure 4*c). Angular velocity is roughly constant during each circular-motion interval (i.e., in each CCW or CW period) and quickly changes sign after CCW-CW switching (*Figure 4*d and Movie S8). Due to the distribution of pili across the cell body, tethering can occur at a pole or

under the body, which leads to cells standing vertically or lying down horizontally to the surface, respectively. We find that standing tethered cells perform a faster circular motion (mean angular speed = 8.5 ± 1.9 rad/s) than lying ones (mean angular speed = 3.0 ± 2.1 rad/s) (*Figure 4*e). For the horizontal cells, different MSHA pili may be used to further anchor the cell to the surface. For example, two horizontally-tethered cells demonstrate different tethered-motion trajectories depending on the location of the anchoring MSHA pilus (*Figure 4-Figure supplement 1*). In addition to the fact that unattached pili may increase the likelihood that the cell will make irreversible attachment, we observe that MSHA pili appear to be able to attach to the surface along their entire length, and not just the tip (Movie S9).

Interestingly, we find that the flagellum of attached cells frequently continues to rotate (Movie S5, after 4.68 s), indicating that even after cell attachment, the flagellar motor is still active for some period. The flagellum will eventually stop rotating after a cell stay long enough on the surface (Movie S10).

RFT-based hydrodynamic models of running and tethered cells

To further understand the landing dynamics of cells, we first employ a resistive force theory (RFT) (*Chen et al., 2000; Magariyama et al., 2002; Magariyama et al., 1995*) for cells in the running phase. This theory predicts a linear relation between v and ω_c, and between v and flagellar rotation rate ω_f (see Methods), as given by:

$$v = \frac{\beta_c \gamma_f}{\alpha_c \beta_f + \alpha_f \beta_f - \gamma_f^2} \omega_c \quad (1)$$

$$v = -\frac{\beta_c \gamma_f}{\alpha_c \beta_c + \alpha_f \beta_c} \omega_f, \quad (2)$$

where α_c, β_c are drag coefficients of cell body, while $\alpha_f, \beta_f, \gamma_f$ are drag coefficients of flagellar filament. These parameters are themselves functions of cell geometry such as cell width and length, flagellar diameter and length, as well as apparent viscosities of solutions in the normal and tangential directions μ_N^* and μ_T^* (see Methods for detailed expressions). Although μ_N^* and μ_T^* are not known exactly, to first order we set them to be equal to the viscosity of the solution, μ. The drag coefficients are then estimated

by applying the parameter values obtained from the measurements in this work and from Magariyama and Kudo (*Magariyama et al., 2002*) (see Table 2). Using equation 1, we estimate $|v/\omega_c|$ to be ~0.5 μm/radian, which agrees well with our experimental measurement. By adjusting μ_T^* while keeping μ_N^* equal to μ, we find that when $\mu_T^* = 0.33*\mu$, the estimated ratio of $|v/\omega_c|$ matches the experimental value. Under this condition, we estimate that $|\omega_f/\omega_c|$ ~10, and $|v/\omega_f|$ ~0.039 μm/radian (or 0.245 μm per revolution); this value is similar to published values for *V. alginolyticus* (*Magariyama et al., 1995*) as well as *E. coli* (*Darnton et al., 2007*).

Then for tethered cells, we utilize a hydrodynamic model (*Bennett et al., 2016*) developed to compare the motion of standing tethered cells and horizontal lying ones (see Methods for further details). We find that for cells that attach to the surface by a pilus located on the pole opposite to the flagellum, the point of surface attachment, flagellar hook stiffness, and flagellar motor torque can affect the preferred tilt angle of cells. Using a hook stiffness of k_h=20 pN·μm in the model, cells move into a preferred standing orientation for flagellar motor torque of Γ=4 pN·μm, whereas cells with motor torque Γ=1 pN·μm are sensitive to the initial angle of attack, as shown in Figure 4f. According to the model, tethered cells can change their preferred tilt angle from lying down (<0.2π) to standing up (~π/2) by increasing motor torque; this suggests that cells could actively adjust their tilt angle during tethered motion through motor-torque control. Compared with horizontal cells, standing cells experience less viscous resistance, due to the shorter trajectory they trace out and the increased average distance between the bacterium and the surface. This could contribute to the experimentally observed faster angular speed of circular motion of standing cells. Even when a cell maintains a particular tilt angle, the angular speed of this tethered motion decreases monotonically as a function of the closest distance between the cell body and the surface (*Figure 4*g).

Role of MSHA pili in cell landing is more apparent in viscous solutions

To further investigate the dependence of MSHA pili function and hence cell landing on viscosity, we compared cell motion behavior obtained in 2% LB, which has a viscosity ~1 cP at 30 ℃ (*Utada et al., 2014*) and in LB+MC, which has a viscosity ~187 cP at 30 ℃, for both WT and △*mshA* cells (*Figure 5* and *Figure 5-Figure supplement 1*).

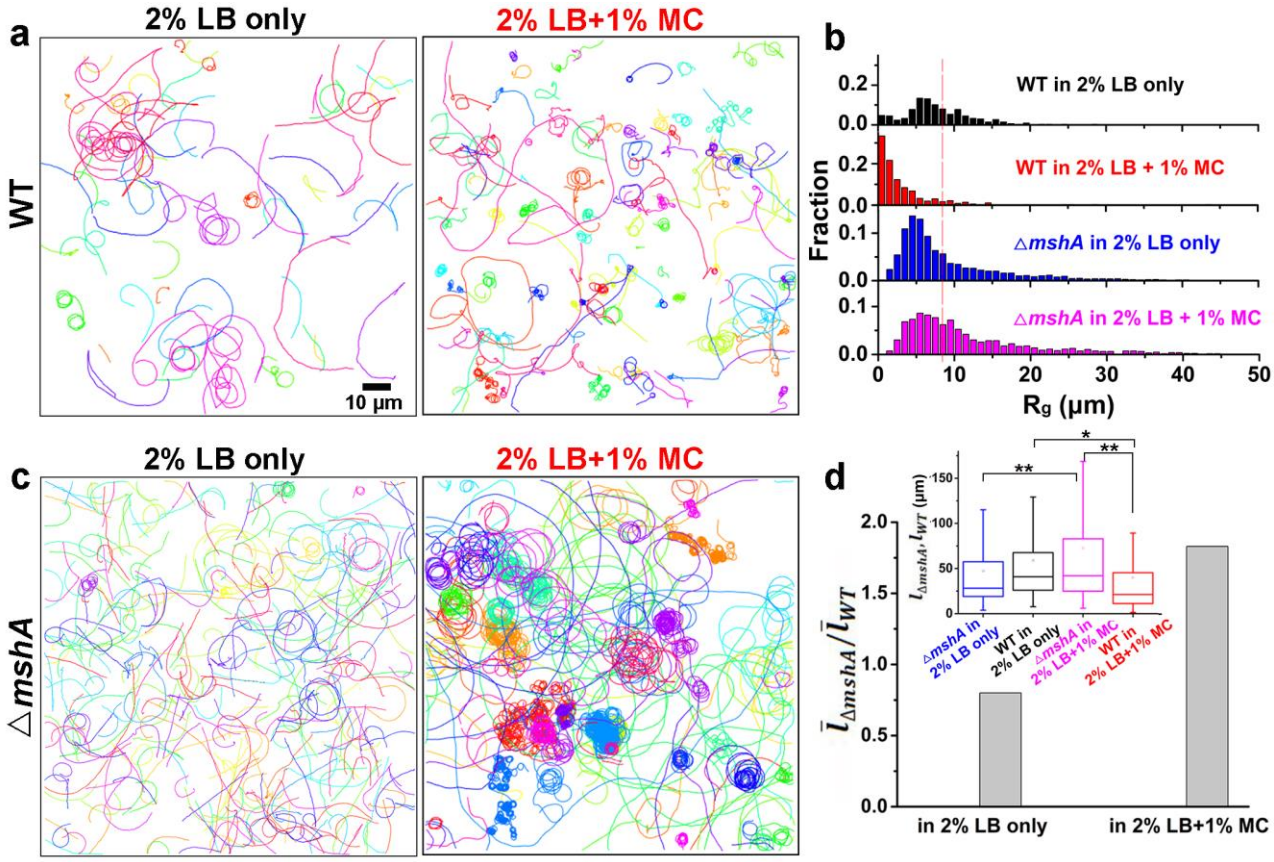

Figure 5. Role of MSHA pili in cell landing is more apparent in viscous solutions. (a) Examples of WT cell trajectories showing both roaming and orbiting motilities in 2% LB only and in 2% LB with 1% MC; (b) Histograms of R_g of WT and △*mshA* in different viscous solutions; (c) Examples of cell trajectories of △*mshA*; (d) The ratio of mean path length between △*mshA* and WT, $\bar{l}_{\Delta mshA}/\bar{l}_{WT}$. The inset shows a box plot summary of path lengths of WT and △*mshA,* where statistical significance was determined with one-way ANOVA followed by Tukey's multiple comparison test comparing the

different groups, using the Prism 5.0 software program (GraphPad Software, La Jolla, CA, USA). (*p < 0.05; **p < 0.01; ***p < 0.001).

Figure 5-Figure supplement 1. Motility characterization of WT and △*mshA* cells in 2% LB only and in 2% LB with 1% MC.

We observe WT cells to demonstrate roaming and orbiting motilities in both solutions (*Figure 5*a). The histograms of deviation angle of each type of motility obtained in the two solutions are also similar (*Figure 5-Figure supplement 1*a and b). These results indicate that roaming and orbiting motilities of cells are robust against viscosity. Although the general motility pattern is similar in both solutions, the motion of cells, as expected, is slowed significantly in LB+MC. The average speed of WT cells for near-surface motion is reduced by ~ 22 times from 86.7 ± 32.9 μm/s (mean ± standard deviation) in 2% LB to 3.8 ± 2.6 μm/s in LB+MC. Similarly, the average speed of △*mshA* cells is also decreased by ~ 12 times from 80.0 ± 15.0 μm/s in 2% LB to 6.5 ± 1.4 μm/s in LB+MC. The slow-down of motion can also be seen clearly from their mean square displacement curves (*Figure 5-Figure supplement 1*c and d), which show similar shape but very different time scales.

However, WT and △*mshA* cells also show differences in their motility behavior in these two solutions. In LB+MC, WT cells tend to land on the surface soon after approaching it (less than one round in orbiting motility) and more tethered motions are observed, which leads to more irregular and tortuous trajectories and smaller R_g for WT cells compared with the case of 2% LB (*Figure 5*b). By contrast, △*mshA* cells show very similar R_g distributions in the two types of solutions (*Figure 5*b). More interestingly, compared with WT, in LB+MC, a large proportion of △*mshA* cells show orbiting for a substantial large number of cycles, as shown in Figure 5c. Quantitatively, this can be seen by the calculated mean path(trajectory) length, $\bar{l}$, which is 39.7 ± 51.2 μm for WT and 72.5 ± 99.1 μm for

314 △*mshA* in LB+MC, whereas the corresponding value in 2% LB is 58.7 ± 63.1 μm for WT and 47.2 ±
315 50.8 μm for △*mshA*. To see how the role of MSHA pili varies with viscosity, we can calculate the ratio
316 of mean path length between △*mshA* and WT, $\bar{l}_{\Delta mshA}/\bar{l}_{WT}$, for each type of solution, which is ~1.8 in
317 LB+MC and ~ 0.8 in 2% LB only, respectively (*Figure 5*d). So loss of MSHA pili results in a more
318 dramatic increase in mean path length in LB+MC than in 2% LB. Together, these results indicate that
319 the role of MSHA as a braking and anchoring machine in cell landing is more apparent in viscous
320 solutions.

321 ## Discussion

322 The first step in *V. cholerae* biofilm formation is the transition from planktonic swimmers to
323 stationary surface attached cells; this process is mediated by the landing process (*Teschler et al., 2015*).
324 In this study, the combination of cell appendage labelling with high-resolution spatio-temporal imaging
325 allows us to quantitatively deconstruct the landing process into three stages: running, lingering, and
326 attaching. During the running phase, cell motion is powered by flagellar rotation, which simultaneously
327 induces a counter-rotation of cell body; this near-surface motion is well described by RFT theory. When
328 swimming cells come to within a distance that is comparable to the length of a typical pilus from a
329 surface, dangling pili may brush against the surface, thereby deflecting the trajectory. Typical MSHA
330 pili are ~0.4-1.2 μm in length. During near surface swimming, cell body rotation actively brings MSHA
331 pili into close proximity with the underlying surface where friction between pili and the surface can slow
332 the cells, or, transient adhesions can be made, which may even arrest cell motion. Here, we make an
333 analogy to the slow-down and stop effected by the brake system of a car. During near-surface swimming,
334 it has been suggested that hydrodynamic forces cause the cell bodies of swimming rod-like bacteria to
335 take on a tilted, non-parallel, orientation to the surface (*Vigeant et al., 2002*). In the case of *P.*
336 *aeruginosa*, whose TFP are distributed with a strong bias toward a particular pole (*Skerker et al., 2001*),

pili-surface contact will depend on which pole is closer to the surface. In contrast, the homogeneous distribution of MSHA pili on *V. cholerae* (see Figure 1d) may be more efficient at slowing such tilted cell bodies by increasing the probability that pili encounter the surface.

If the contact-induced adhesion between MSHA pili and the surface is sufficiently strong to arrest forward motion, the cell will either pause or commence tethered motion centered about the point-of-adhesion. Our hydrodynamic model shows that the angular speed of tethered motion decreases monotonically as the cell is brought closer to the surface (*Figure 4*g). This suggests that for cells demonstrating tethered motion, a progressive twisting of the surface-attached pilus fiber during the circular motion of cells may gradually cause the circular motion to stop by pulling the cell body ever closer to the surface. Although twitching has not be observed in *V. cholerae*, this is one mechanism by which retraction-like dynamics may be achieved (*Charles et al., 2019*), possibly in tandem with actual retraction of MSHA pili, which has been shown recently in a different strain of *V. cholera* (*Floyd et al., 2020*). Under our conditions, we have not observed MSHA pili retraction events nor have we seen bacterial cells that gradually acquire fluorescence when only maleimide dyes were used. These results are consistent since in bacteria where pilus retraction does occur, such as in the TAD pili of *Caulobacter crescentus* (*Ellison et al., 2017*), ChiRP pili of *V. cholera* (*Ellison et al., 2018*), and TFP of *P. aeruginosa* (*Skerker et al., 2001*), the cell body gradually becomes fluorescent due to internalization of labeled pili by retraction. Such phenotypical differences may be due to the different experimental conditions used in each study and require more work to fully elucidate.

In addition to possible hydrodynamical effects, our observation that MSHA pili are able to adhere to surfaces along their entire length highlights their versatility and likely increases the chances of the formation of a cell-surface attachment. The ability to adhere not only at the distal tip, contrasts with the TFP of *P. aeruginosa* (*Skerker et al., 2001*) and ChiRP pili of *V. cholerae* (*Ellison et al., 2018*) who

show the pilus-subject interactions mainly mediated by the pilus tip. Thus, for *V. cholerae*, the strength of adhesion between a cell and a surface that is mediated by an individual MSHA pilus appears to be more complicated to model with a single point of attachment. Rather, cells can enhance the adhesion strength by increasing both the length and the number of the MSHA pilus adhered to the surface. This will facilitate cells to become irreversibly attached.

Similar running and lingering phases for cells near surface motion has also been reported in enterohaemorrhagic *E. coli* (EHEC) cells (*Perez Ipiña et al., 2019*), where results suggested that by choosing the optimal transition rates, EHEC bacterial diffusivity is maximized and the surface exploration efficiency is greatly improved. In a future work, it will be interesting to apply similar analysis in *V. cholerae*.

In this study, the data collection of *V. cholerae* cells was performed mainly in the viscous solution of LB+MC. The viscous solution used in these experiments simultaneously slows cell motion, which enables the capture of the dynamics of the fluorescently labelled MSHA pili and flagellar, while simulating the highly viscous environment that *V. cholerae* cells encounter in the mucus layer of animal intestines. In such viscous environments, Millet *et al.* (*Millet et al., 2014*) observed considerable differences of bacterial localization in different parts of small intestine and found that *V. cholerae* motility exhibits a regiospecific influence on colonization, indicating viscous intestinal mucin is a key factor limiting colonization. In this work, by direct visualization of pili and flagellum of cells during their landing process in LB+MC, we find that *V. cholerae* cells can move well in this highly viscous solution under our conditions. Moreover, we show that the effect of MSHA pili as a braking and anchoring machine on cell landing is more apparent in LB+MC than in 2% LB only, suggesting that MSHA pili might play an even more important role for cell surface attachment in viscous environments such as in small intestines.

To summarize, in this work, using fluorescence imaging with labeled pili and flagellum, we show a comprehensive picture of the landing dynamics of *V. cholerae* cells in viscous environments and provide a direct observational evidence exhibiting the role of MSHA pili during cell landing. We hope this can shed insights into the prevention and control of *V. cholerae* infections.

Materials and methods

Bacterial strains

Bacterial strains used in this study are listed in Table 1. Plasmids and primers used in this study are listed in Table S1. *V. cholerae* El Tor C6706 (*Joelsson et al., 2006*) was used as a parental strain in this study. C6706 and mutants were grown at 30 °C or 37 °C in Luria-Bertani (LB) supplemented with 100 μg/mL streptomycin, 50 μg/mL kanamycin, 1 μg/mL chloromycetin where appropriate. *E. coli* strains harboring plasmids were grown at 37 °C in LB supplemented with 100 μg/mL ampicillin. The optical densities of bacterial cultures were measured at 600 nm (OD_{600}) using a UV-vis spectrophotometer.

Table 1. Strains used in this study

Strain	Description	Source or reference
parent	C6706 Sm^R	(*Joelsson et al., 2006*)
Δ*mshA*	C6706 Sm^R, VC1807::Cm^R, *mshA* knockout	This study
Δ*flaA*	C6706 Sm^R, VC1807::Cm^R, *flaA* knockout	This study
$MshA^{T70C}$	C6706 Sm^R, VC1807::Km^R, MshAT70C	(*Ellison et al., 2017*)
$FlaA^{A106C}$	C6706 Sm^R, VC1807::Cm^R, FlaAA106C	This study
$FlaA^{S107C}$	C6706 Sm^R, VC1807::Cm^R, FlaAS107C	This study
$FlaA^{A106CS107C}$	C6706 Sm^R, VC1807::Cm^R, FlaAA106CS107C	This study
$FlaA^{E332C}$	C6706 Sm^R, VC1807::Cm^R, FlaAE332C	This study
$FlaA^{G23C}$	C6706 Sm^R, VC1807::Cm^R, FlaAG23C	This study
$FlaA^{N26C}$	C6706 Sm^R, VC1807::Cm^R, FlaAN26C	This study

FlaA^{N83C}	C6706 Sm^{R}, VC1807::Cm^{R}, FlaAN83C	This study
FlaA^{S325C}	C6706 Sm^{R}, VC1807::Cm^{R}, FlaAS325C	This study
FlaA^{S87C}	C6706 Sm^{R}, VC1807::Cm^{R}, FlaAS87C	This study
FlaA^{S376C}	C6706 Sm^{R}, VC1807::Cm^{R}, FlaAS376C	This study
FlaA^{V117C}	C6706 Sm^{R}, VC1807::Cm^{R}, FlaAV117C	This study
MshA^{T70C}, Δ*flaA*	C6706 Sm^{R}, VC1807::Km^{R}, *flaA* knockout	This study
MshA^{T70C}, FlaA^{A106C}	C6706 Sm^{R}, VC1807::Km^{R}, FlaAA106C	This study
MshA^{T70C}, FlaA^{S107C}	C6706 Sm^{R}, VC1807::Km^{R}, FlaAS107C	This study
MshA^{T70C}, FlaA^{A106CS107}	C6706 Sm^{R}, VC1807::Km^{R}, FlaAA106CS107C	This study

Flagellin and pilin mutagenesis

Following the protocol in Ellison *et al*. (*Ellison et al., 2019; Ellison et al., 2017*), we first predicted 10 amino acid residues in *V. cholerae* flagellin FlaA for cysteine replacement. Then the *flaA* knockout and FlaA sequences containing the FlaAA106C, FlaAS107C, FlaAA106CS107C, FlaAE332C, FlaAG23C, FlaAN26C, FlaAN83C, FlaAS325C, FlaAS87C, FlaAS376C, FlaAV117C knock-in were constructed using the MuGENT method (*Dalia et al., 2014*). The FlaAA106C, FlaAS107C, and FlaAA106CS107C knock-in were constructed by cloning the fragment into the suicide vector pWM91 containing a *sacB* counter-selectable marker (*Metcalf et al., 1996*). The plasmids were introduced into *V. cholerae* by conjugation and mutations were selected for double homologous recombination events. The MshAT70C mutation can be successfully labeled with thiol-reactive maleimide dyes has been described previously (*Ellison et al., 2017*), and MshAT70C was constructed using the MuGENT method to light MSHA pilus. All mutants were confirmed by DNA sequencing.

Hemagglutination assays

Mannose-sensitive hemagglutination by *V. cholerae* was measured as described previously (*Gardel et al., 1996*). Briefly, bacteria were grown to the mid-logarithmic phase in LB medium. Initial

concentrations of approximately 10^{10} CFU/mL were two-fold diluted with KRT buffer in U-bottomed wells of 96-sample microtiter dishes. Sheep erythrocytes were washed in PBS and resuspended in KRT buffer for a final concentration of 10% vol/vol. Equivoluminal erythrocyte were added into serially diluted bacterial suspensions and the plates were gently agitated at room temperature for 1 min. Samples were checked for hemagglutination after 2 h at room temperature (RT).

The results of the Hemagglutination assay test show that MshAT70C displays similar behavior to WT, which indicates that the point mutation in MSHA does not affect MSHA pilus function (*Figure 1-Figure supplement 2*).

Preparation of viscous solution and viscosity measurements

To change the solution viscosity, methyl cellulose (MC) (M20, 4000 cp, Solarbio, China) solutions were prepared by dissolving 1% (wt/vol) MC in 2% LB motility medium (containing 171 mM NaCl). The shear viscosity measurements were performed on a Physica MCR 302 rheometer (Anton Paar, Germany) at 30 °C.

Cell imaging

For the *V. cholerae* motility observation in 2% LB without MC, overnight cultures in LB were resuspended and diluted with 2% LB to an OD_{600} ranging from 0.01-0.03. Then the bacterial suspension was injected into a flow cell, which contained the same media. Imaging was performed using a Phantom V2512 high-speed camera (Vision Research, USA) collecting ~200 000 bright-field images at 5 ms resolution with a 100× oil objective on a Leica DMi8 inverted microscope (Leica, Germany).

For the *V. cholerae* motility observation in 2% LB with 1% MC (henceforth, this medium is referred to LB+MC), overnight cultures in LB were resuspended and diluted with LB+MC to a final OD_{600} of 0.01-0.03. Then, the bacteria were incubated at 37°C for 20 min to allow them to adapt to the new environment and were then used immediately. Bacteria samples were pipetted onto standard microscope

slides with a 8 mm diameter spot and then were sealed with a coverslip using a 1 mm thick secure spacer. Imaging was performed using EMCCD camera (Andor iXon Ultra 888) collecting ~10 000 bright-field images at 90 ms resolution.

Cell-tracking and analysis

The images were preprocessed using a combination of software and algorithms adapted from the methods described (*Lee et al., 2016; Utada et al., 2014; Zhao et al., 2013*) and written in MATLAB R2015a (Mathworks) by subtracting the background, scaling, smoothing and thresholding. After image processing in this way, the bacteria appear as bright regions. The bacteria shape was fit with a spherocylinder. Then the geometric information of the cell, such as location of the centroid and two poles, and the length and width of the bacterium were collected. Trajectory reconstruction was also achieved for further analysis.

The motility parameters(*Utada et al., 2014*), such as instantaneous speed, deviation angle, radius of gyration (R_g) and MSD were calculated to further characterize the near-surface motility of *V. cholerae*. The instantaneous speed was calculated via $|r_{i+1}-r_i|/\triangle t$, where r_i is the cell position vector in frame i and $\triangle t$ is the time interval between two consecutive frames. The deviation angle of cell motion is defined as the angle between its cell body axis and the direction of motion. The radius of gyration, R_g, is a statistical measure of the spatial extent of the domain of motion given by an ensemble of points that define a trajectory(*Rubenstein, 2003*). The square of this quantity is defined as $R_g^2 = \frac{1}{N}\sum_{i=1}^{N}(\vec{R}_i - \vec{R}_{cm})^2$, where N is the number of points in the tracked trajectory, $\vec{R}_i$ is the position vector corresponding to the i-th point on the trajectory, $\vec{R}_{cm}$ is the position vector of the center-of-mass. The MSD of cells was calculated via $\langle \Delta r^2(\tau) \rangle = \langle [r(t+\tau) - r(t)]^2 \rangle$, where $r(t)$ is the position vector of a cell at time t, and τ represents the time lag. The MSD provides information on the average displacement between points in the motility trajectory separated by a fixed time lag.

458 To calculate the persistence lengths of pili(*Gibiansky et al., 2010; Samad et al., 2017*), we first
459 extracted the centerline of a broken pilus through the morphological thinning skeleton transformation.
460 Second, we acquired the coordinates of all points on this centerline. Then, persistence length L_P of a
461 broken pilus was calculated according to $\langle \cos\theta_l \rangle = e^{-l/L_p}$, where l is the distance travelled along the
462 curve, θ_l is the angle between tangents to the path at a separation distance of l apart, and the angled
463 brackets indicate ensemble and time averages .

464 **MSHA pilus labeling, imaging, and quantification**

465 Pilin labeling was achieved using Alexa Fluor 488 C5 Maleimide (AF488-mal; ThermoFisher
466 Scientific, cat. no. A10254) or Alexa Fluor 546 C5 Maleimide (AF546-mal; ThermoFisher Scientific,
467 cat. no. A10258), which were dissolved in DMSO, aliquoted, and stored at -20˚C while being protected
468 from light.

469 *V. cholerae* cultures were grown to mid-log phase (OD_{600} 0.8-1.5) before labeling. ~100 µL of culture
470 was mixed with dye at a final concentration of 25 µg/mL(*Ellison et al., 2017*) and incubated at RT for 5
471 min in the dark. Labeled cultures were harvested by centrifugation (900×g, 5 min) and washed twice
472 with PBS, resuspended in 200 µL PBS and imaged immediately. Images were collected using an
473 EMCCD camera on a Leica DMi8 inverted microscope equipped with an Adaptive Focus Control
474 system. The fluorescence of cells labeled with AF488-mal and AF546-mal were detected with FITC and
475 Rhod filter, respectively. The cell bodies were imaged using phase contrast microscopy.

476 To quantify the number of MSHA pili per cell and cell length, imaging was done under 0.2% PBS
477 gellan gum pads. The cell lengths were measured using ImageJ.

478 We used AF546-mal and AF488-mal, in turn, for the two-color labeling to observe the growth of pili.
479 We first, labeled log-phase cells with AF546-mal for the primary staining by incubating for 20 min,
480 followed by two successive washes in PBS by centrifugation. The cells were then resuspended in LB

and incubated for an additional 40 min at 30 °C. For the secondary staining, we incubated the cells in AF488-mal for 5 min, washed twice with PBS, and then imaged the cells immediately using phase contrast, FITC, and RhoD channels.

Fluorescence movie acquisition of MSHA pilus-labelled cells motility in LB + MC

The labeled cells were centrifugated, resuspended in ~20 µL PBS, and then diluted in 500 µL of the viscous solution of LB + MC. The solution was then immediately pipetted onto a standard microscope slides. Fluorescence images were acquired at 130 ms intervals for a total of about 2-5 min. After a few minutes of fluorescence imaging, most cells in the field of view have attached to the surface, while the fluorescence was bleached due to the continuous exposure. We recorded images from different locations to capture new instances of bacterial movement and adhesion events.

Calculation of swimming speed of cell and rotation rate of cell body using an RFT model

To calculate the swimming speed of cell ν and rotation rate of cell body ω_c, we employed a modified resistive force theory (RFT) proposed by Magariyama and Kudo(*Magariyama et al., 2002*), which gives ν, ω_c and rotation rate of flagellum ω_f as follows:

$$v = K_0 \beta_c \gamma_f \tag{3}$$

$$\omega_f = -K_0(\alpha_c \beta_c + \alpha_f \beta_c) \tag{4}$$

$$\omega_c = K_0(\alpha_c \beta_f + \alpha_f \beta_f - \gamma_f^2) \tag{5}$$

$$K_0 = 1/\left[\frac{\beta_c(\alpha_c \beta_f + \alpha_f \beta_f - \gamma_f^2)}{T_0} - \frac{\alpha_c \beta_c + \alpha_c \beta_f + \alpha_f \beta_c + \alpha_f \beta_f - \gamma_f^2}{\omega_0}\right] \tag{6}$$

Here, α_c and β_c are drag coefficients of cell body; α_f, β_f and γ_f are drag coefficients of flagellum; T_0 is flagellar motor torque at rotation rate of 0, and ω_0 is flagellar rotation rate at motor torque of 0. The drag coefficients can be expressed as follows:

$$\alpha_c = -6\pi\mu_N^* a\left\{1 - \frac{1}{5}\left(1 - \frac{b}{a}\right)\right\} \tag{7}$$

$$\beta_c = -8\pi\mu_T^* a^3\left\{1 - \frac{3}{5}\left(1 - \frac{b}{a}\right)\right\} \tag{8}$$

$$\alpha_f = \frac{2\pi\mu_N^* L}{(log[d/2p] + 1/2)(4\pi^2 r^2 + p^2)}\left(8\pi^2 r^2 + \frac{\mu_T^*}{\mu_N^*}p^2\right) \quad (9)$$

$$\beta_f = \frac{2\pi\mu_N^* L}{(log[d/2p] + 1/2)(4\pi^2 r^2 + p^2)}\left(2p^2 + \frac{\mu_T^*}{\mu_N^*}4\pi^2 r^2\right)r^2 \quad (10)$$

$$\gamma_f = \frac{2\pi\mu_N^* L}{(log[d/2p] + 1/2)(4\pi^2 r^2 + p^2)}\left(2 - \frac{\mu_T^*}{\mu_N^*}\right)(-2\pi r^2 p) \quad (11)$$

Here, μ_T^* and μ_N^* are apparent viscosities in the normal and tangential directions. *a*, *b*, *d*, *p*, *L* and *r* are cell geometric parameters. Their meanings and all the parameter values used in this work are shown in Table 2.

Specifically, we measured the cell width and length of *V. cholerae* to be 0.94 ± 0.10 μm and 2.76 ± 0.63 μm, respectively (N=1900 cells). Although μ_N^* and μ_T^* are not known exactly, to first order we set them to be equal to the viscosity of the solution, μ, which is 0.187 Pa·s for LB + MC at 30 °C. We then use the values from Magariyama and Kudo (*Magariyama et al., 2002*) to obtain estimates for the remaining parameters to calculate the drag coefficients used in equation 1 and 2 (see Table 2).

Table 2. Parameters used in the model

Symbol	Parameter	Average (μm)	SD (μm)
2*a*	Cell width	0.94*	0.10
2*b*	Cell length	2.76*	0.63
2*d*	Diameter of flagellar filament	0.032†	
L	Length of flagellar filament	5.02†	
p	Pitch of flagellar helix	1.58†	
r	Radius of flagellar helix	0.14†	

*Values measured in this study; †Values from reference (*Magariyama et al., 2002; Magariyama et al., 1995*)

520 **Hydrodynamic model of tethered bacteria**

521 To investigate the motion of tethered cells, we use a modified version of the RFT-based
522 hydrodynamic model of *V. cholera* (*Bennett et al., 2016*), which models the flagellum as a helical
523 filament and the curved body as a thicker half-helix. The body and the flagellum are connected by the
524 flagellar hook, modelled as a torsional spring that favors alignment between the body and flagellum. In
525 the original model (*Bennett et al., 2016*), the cell is constrained to the surface by a section of the
526 flagellum; here, we consider a surface constraint via a pilus at the pole opposite the flagellum which we
527 model by allowing the cell to rotate about its pole at a point at height h above the surface. A flagellar
528 motor torque is exerted between the flagellum and the body, we use RFT coefficients from the literature
529 for a helix near a surface, and a torque free condition on the cell to calculate the components of
530 rotational velocity for the body and the flagellum. The other modifications from the original model
531 (*Bennett et al., 2016*) are use of the geometric parameters given in Table 2 and a viscosity of 0.187 Pa·s
532 to compare with experiments in LB + MC at 30 °C.
533

Acknowledgements

We thank Zhanglin Hou for his help with scientific discussions.

Additional information

Funding

Funder	Grant reference number	Author
National Key R&D Program of China	2018YFA0902102	Kun Zhao, Wenchao Zhang, Chunying Feng
National Natural Science Foundation of China (NSFC)	31770132	Zhi Liu, Mei Luo
National Natural Science Foundation of China (NSFC)	81572050	Zhi Liu, Mei Luo
National Natural Science Foundation of China (NSFC)	21621004	Kun Zhao, Wenchao Zhang, Chunying Feng
University of Bristol Vice-Chancellor's Fellowship		Rachel R. Bennett
Grant in aid for Young Scientists (B) from the Japanese Society for the Promotion of Science (JSPS)	17K15410	Andrew S. Utada

The funders had no role in study design, data collection and interpretation, or the decision to submit the work for publication.

Author contributions

K.Z. and Z.L. conceived the project. K.Z., Z.L. and A.S.U. designed studies. W.Z. and M.L. performed experimental measurements. W.Z., A.S.U. and K.Z. performed image analysis. C.F. helped in collecting experimental data. M.L. and Z.L. constructed strains. R.R.B. designed the hydrodynamic model and performed computer simulations. W.Z., M.L., R.R.B., A.S.U., Z.L. and K.Z. wrote the paper. All authors discussed the results and commented on the manuscript.

Conflict of interest The authors declare that they have no conflict of interest.

Additional files

Supplementary file: including Supplementary figures, tables and movie legends.

Transparent reporting form

Data availability

Source data files and MATLAB code have been provided for Figures 1-5.

References

Almagromoreno S, Pruss K, Taylor RK. 2015. Intestinal colonization dynamics of *Vibrio cholerae*. *PLoS Pathogens* **11**: e1004787. DOI:10.1371/journal.ppat.1004787, PMID: 25996593

Bennett RR, Lee CK, De AJ, Nealson KH, Yildiz FH, O'Toole GA, Wong GC, Golestanian R. 2016. Species-dependent hydrodynamics of flagellum-tethered bacteria in early biofilm development. *Journal of the Royal Society Interface* **13**:20150966. DOI: 10.1098/rsif.2015.0966, PMID: 26864892

Blair KM, Turner L, Winkelman JT, Berg HC, Kearns DB. 2008. A molecular clutch disables flagella in the *Bacillus subtilis* biofilm. *Science* **320**: 1636-1638. DOI:10.1126/science.1157877, PMID: 18566286

Charles N, Gazzola M, Mahadevan L. 2019. Topology, geometry, and mechanics of strongly stretched and twisted filaments: solenoids, plectonemes, and artificial muscle fibers. *Physical Review Letters* **123**: 208003. DOI: 10.1103/PhysRevLett.123.208003, PMID: 31809094

Chen X, Berg HC. 2000. Torque-speed relationship of the flagellar rotary motor of Escherichia coli. *Biophysical Journal* **78**: 1036-1041. DOI: 10.1016/S0006-3495(00)76662-8, PMID: 10653817

Dalia AB, McDonough E, Camilli A. 2014. Multiplex genome editing by natural transformation. *PNAS* **111**: 8937-8942. DOI: 10.1073/pnas.1406478111, PMID: 24889608

Darnton NC, Turner L, Rojevsky S, Berg HC. 2007. On torque and tumbling in swimming *Escherichia coli*. *Journal of Bacteriology* **189**: 1756-1764. DOI: 10.1128/JB.01501-06, PMID: 17189361

Donlan RM, Costerton JW. 2002. Biofilms: survival mechanisms of clinically relevant microorganisms. *Clinical Microbiology Reviews* **15**: 167-193. DOI: 10.1128/cmr.15.2.167-193.2002, PMID: 11932229

Ellison CK, Dalia TN, Dalia AB, Brun YV. 2019. Real-time microscopy and physical perturbation of bacterial pili using maleimide-conjugated molecules. *Nat Protoc* **14**: 1803-1819. DOI: 10.1038/s41596-019-0162-6, PMID: 31028374

577 Ellison CK, Dalia TN, Vidal Ceballos A, Wang JC-Y, Biais N, Brun YV, Dalia AB. 2018. Retraction of
578 DNA-bound type IV competence pili initiates DNA uptake during natural transformation in *Vibrio*
579 *cholerae*. *Nature Microbiology* **3**: 773-780. DOI: 10.1038/s41564-018-0174-y, PMID: 29891864
580 Ellison CK, Kan J, Dillard RS, Kysela DT, Ducret A, Berne C, Hampton CM, Ke Z, Wright ER, Biais N.
581 2017. Obstruction of pilus retraction stimulates bacterial surface sensing. *Science* **358**: 535-538.
582 DOI: 10.1126/science.aan5706, PMID: 29074778
583 Floyd KA, Lee CK, Xian W, Nametalla M, Valentine A, Crair B, Zhu S, Hughes HQ, Chlebek JL, Wu DC,
584 Hwan Park J, Farhat AM, Lomba CJ, Ellison CK, Brun YV, Campos-Gomez J, Dalia AB, Liu J, Biais N,
585 Wong GCL et al. 2020. C-di-GMP modulates type IV MSHA pilus retraction and surface attachment in
586 *Vibrio cholerae*. *Nature Communication* **11**: 1549. DOI: 10.1038/s41467-020-15331-8,
587 PMID: 32214098
588 Friedlander RS, Vlamakis H, Kim P, Khan M, Kolter R, Aizenberg J. 2013. Bacterial flagella explore
589 microscale hummocks and hollows to increase adhesion. *PNAS* **110**: 5624-5629.
590 DOI: 10.1073/pnas.1219662110, PMID: 23509269
591 Gardel CL, Mekalanos JJ. 1996. Alterations in *Vibrio cholerae* motility phenotypes correlate with changes
592 in virulence factor expression. *Infect Immun* **64**: 2246-2255. PMID:8675334
593 Gibiansky ML, Conrad JC, Jin F, Gordon VD, Motto DA, Mathewson MA, Stopka WG, Zelasko DC,
594 Shrout JD, Wong GC. 2010. Bacteria use type IV pili to walk upright and detach from surfaces. *Science*
595 **330**: 197. DOI: 10.1126/science.1194238, PMID: 20929769
596 Guttenplan SB, Kearns DB. 2013. Regulation of flagellar motility during biofilm formation. *FEMS*
597 *Microbiology Reviews* **37**: 849-871. DOI: 10.1111/1574-6976.12018, PMID: 23480406

598 Higashi DL, Lee SW, Snyder A, Weyand NJ, Bakke A, So M. 2007. Dynamics of *Neisseria gonorrhoeae*
599 attachment: microcolony development, cortical plaque formation, and cytoprotection. *Infection and*
600 *Immunity* **75**: 4743-4753. DOI: 10.1128/IAI.00687-07, PMID: 17682045
601 Joelsson A, Liu Z, Zhu J. 2006. Genetic and phenotypic diversity of quorum-sensing systems in clinical
602 and environmental isolates of *Vibrio cholerae*. *Infect Immun* **74**: 1141-1147.
603 DOI: 10.1128/IAI.74.2.1141-1147.2006, PMID: 16428762
604 Kaper J B MJG, Levine M M. 1995. Cholera. *Clinical Microbiology Reviews* **8**: 48-86. PMID: 7704895
605 Kirn TJ, Lafferty MJ, Sandoe CMP, Taylor RK. 2000. Delineation of pilin domains required for bacterial
606 association into microcolonies and intestinal colonization by *Vibrio cholerae*. *Molecular Microbiology*
607 **35**: 896-910. DOI: 10.1046/j.1365-2958.2000.01764.x, PMID: 10692166
608 Krukonis ES, Dirita VJ. 2003. From motility to virulence: Sensing and responding to environmental
609 signals in *Vibrio cholerae*. *Current Opinion in Microbiology* **6**: 186-190. DOI: 10.1016/s1369-
610 5274(03)00032-8, PMID: 12732310
611 Lai SK, Wang Y-Y, Wirtz D, Hanes J. 2009. Micro-and macrorheology of mucus. *Advanced Drug*
612 *Delivery Reviews* **61**: 86-100. DOI: 10.1016/j.addr.2008.09.012, PMID: 19166889
613 Lee CK, Kim AJ, Santos GS, Lai PY, Lee SY, Qiao DF, De AJ, Young TD, Chen Y, Rowe AR. 2016.
614 Evolution of cell size homeostasis and growth rate diversity during initial surface colonization of
615 *Shewanella oneidensis*. *Acs Nano* **10**:9183-9192. DOI: 10.1021/acsnano.6b05123, PMID: 27571459
616 Lee J-H, Rho JB, Park K-J, Kim CB, Han Y-S, Choi SH, Lee K-H, Park S-J. 2004. Role of flagellum and
617 motility in pathogenesis of *Vibrio vulnificus*. *Infection and Immunity* **72**: 4905-4910.
618 DOI: 10.1128/IAI.72.8.4905-4910.2004, PMID: 15271959

619 Magariyama Y, Sugiyama S, Muramoto K, Kawagishi I, Imae Y, Kudo S. 1995. Simultaneous
620 measurement of bacterial flagellar rotation rate and swimming speed. *Biophysical Journal* **69**: 2154-
621 2162. DOI: 10.1016/S0006-3495(95)80089-5, PMID: 8580359
622 Magariyama Y, Kudo S. 2002. A mathematical explanation of an increase in bacterial swimming speed
623 with viscosity in linear-polymer solutions. *Biophysical Journal* **83**: 733-739. DOI: 10.1016/S0006-
624 3495(02)75204-1, PMID: 12124260
625 Maier B, Potter L, So M, Seifert HS, Sheetz MP. 2002. Single pilus motor forces exceed 100 pN. *PNAS* **99**:
626 16012-16017. DOI: 10.1073/pnas.242523299, PMID: 12446837
627 Meibom KL, Li XB, Nielsen AT, Wu CY, Roseman S, Schoolnik GK. 2004. The *Vibrio cholerae* chitin
628 utilization program. *PNAS* **101**: 2524-2529. DOI: 10.1073/pnas.0308707101, PMID: 14983042
629 Metcalf WW, Jiang W, Daniels LL, Kim SK, Haldimann A, Wanner BL. 1996. Conditionally replicative
630 and conjugative plasmids carrying lacZ alpha for cloning, mutagenesis, and allele replacement in
631 bacteria. *Plasmid* **35**: 1-13. DOI: 10.1006/plas.1996.0001, PMID: 8693022
632 Millet YA, Alvarez D, Ringgaard S, von Andrian UH, Davis BM, Waldor MK. 2014. Insights into *Vibrio*
633 *cholerae* intestinal colonization from monitoring fluorescently labeled bacteria. *PLoS Pathogens* **10**:
634 e1004405. DOI: 10.1371/journal.ppat.1004405, PMID: 25275396
635 Nakane D, Nishizaka T. 2017. Asymmetric distribution of type IV pili triggered by directional light in
636 unicellular cyanobacteria. *PNAS* **114**: 6593-6598. DOI: 10.1073/pnas.1702395114, PMID: 28584115
637 O'Toole GA, Kolter R. 1998. Flagellar and twitching motility are necessary for *Pseudomonas aeruginosa*
638 biofilm development. *Molecular Microbiology* **30**: 295–304. DOI: 10.1046/j.1365-
639 2958.1998.01062.x, PMID: 9791175
640 Perez Ipiña E, Otte S, Pontier-Bres R, Czerucka D, Peruani F. 2019. Bacteria display optimal transport
641 near surfaces. *Nature Physics* **15**: 610-615. DOI: 10.1038/s41567-019-0460-5

642 Piepenbrink KH, Sundberg EJ. 2016. Motility and adhesion through type IV pili in Gram-positive bacteria.
643 *Biochemical Society Transactions* **44**: 1659. DOI: 10.1042/BST20160221, PMID: 27913675
644 Pratt LA, Kolter R. 1998. Genetic analysis of *Escherichia coli* biofilm formation: roles of flagella, motility,
645 chemotaxis and type I pili. *Molecular Microbiology* **30**: 285-293. DOI: 10.1046/j.1365-
646 2958.1998.01061.x, PMID: 9791174
647 Reguera G, Kolter R. 2005. Virulence and the environment: a novel role for *Vibrio cholerae* toxin-
648 coregulated pili in biofilm formation on chitin. *Journal of Bacteriology* **187**: 3551-3555.
649 DOI: 10.1128/JB.187.10.3551-3555.2005, PMID: 15866944
650 Renault TT, Abraham AO, Bergmiller T, Paradis G, Rainville S, Charpentier E, Guet CC, Tu Y, Namba K,
651 Keener JP. 2017. Bacterial flagella grow through an injection-diffusion mechanism. *Elife* **6:** e23136.
652 DOI: 10.7554/eLife.23136, PMID: 28262091
653 Rubenstein MC, R. H. 2003. Polymer Physics. *Oxford University Press*: 60-66.
654 Samad T, Billings N, Birjiniuk A, Crouzier T, Doyle PS, Ribbeck K. 2017. Swimming bacteria promote
655 dispersal of non-motile staphylococcal species. *The ISME journal* **11**: 1933.DOI: 10.1038/ismej.2017.23,
656 PMID: 28398350
657 Silva AJ, Benitez JA. 2016. *Vibrio cholerae* biofilms and Cholera pathogenesis. *Plos Negl Trop Dis* **10**:
658 e0004330. DOI: 10.1371/journal.pntd.0004330, PMID: 26845681
659 Skerker JM, Berg HC. 2001. Direct observation of extension and retraction of type IV pili. *PNAS* **98**:
660 6901-6904. DOI: 10.1073/pnas.121171698, PMID: 11381130
661 Talà L, Fineberg A, Kukura P, Persat A. 2019. *Pseudomonas aeruginosa* orchestrates twitching motility
662 by sequential control of type IV pili movements. *Nature microbiology* **4**: 774-780.
663 DOI: 10.1038/s41564-019-0378-9, PMID: 30804544

664 Teschler JK, Zamoranosánchez D, Utada AS, Warner CJ, Wong GC, Linington RG, Yildiz FH. 2015.
665 Living in the matrix: assembly and control of *Vibrio cholerae* biofilms. *Nature Reviews Microbiology*
666 **13**: 255-268. DOI: 10.1038/nrmicro3433, PMID: 25895940
667 Thelin KH, Taylor RK. 1996. Toxin-coregulated pilus, but not mannose-sensitive hemagglutinin, is
668 required for colonization by *Vibrio cholerae* O1 El Tor biotype and O139 strains. *Infection & Immunity*
669 **64**: 2853-2856.
670 Tsou A, Frey E, Hsiao A, Liu Z, Zhu J. 2008. Coordinated regulation of virulence by quorum sensing and
671 motility pathways during the initial stages of *Vibrio cholerae* infection. *Communicative & integrative*
672 *biology* **1**: 42-44. DOI: 10.4161/cib.1.1.6662, PMID: 19704787
673 Utada AS, Bennett RR, Fong JC, Gibiansky ML, Yildiz FH, Golestanian R, Wong GC. 2014. *Vibrio*
674 *cholerae* use pili and flagella synergistically to effect motility switching and conditional surface
675 attachment. *Nature Communication* **5**: 4913. DOI: 10.1038/ncomms5913, PMID: 25234699
676 Vigeant MA, Ford RM, Wagner M, Tamm LK. 2002. Reversible and irreversible adhesion of motile
677 Escherichia coli cells analyzed by total internal reflection aqueous fluorescence microscopy. *Applied &*
678 *Environmental Microbiology* **68**: 2794-2801. DOI: 10.1128/aem.68.6.2794-2801.2002, PMID:
679 12039734
680 Watnick PI, Kolter R. 1999. Steps in the development of a *Vibrio cholerae* El Tor biofilm. *Molecular*
681 *Microbiology* **34**: 586-595. DOI: 10.1046/j.1365-2958.1999.01624.x, PMID: 10564499
682 Yildiz FH, Visick KL. 2009. Vibrio biofilms: so much the same yet so different. *Trends in Microbiology*
683 **17**: 109-118. DOI: 10.1016/j.tim.2008.12.004, PMID: 19231189
684 Zhao K, Tseng BS, Beckerman B, Jin F, Gibiansky ML, Harrison JJ, Luijten E, Parsek MR, Wong GC.
685 2013. Psl trails guide exploration and microcolony formation in *Pseudomonas aeruginosa* biofilms.
686 *Nature* **497**: 388-391. DOI: 10.1038/nature12155, PMID: 23657259

Supplementary information for

Crash landing of *Vibrio cholerae* by MSHA pili-assisted braking and anchoring in a viscous environment

Wenchao Zhang[1,#], Mei Luo[2,#], Chunying Feng[1], Rachel R. Bennett[3,*], Andrew S. Utada[4,*], Zhi Liu[2,*], Kun Zhao[1,*]

[1] *Frontier Science Center for Synthetic Biology and Key Laboratory of Systems Bioengineering (Ministry of Education), School of Chemical Engineering and Technology, Tianjin University, Tianjin, P.R. China*

[2] *Department of Biotechnology, College of Life Science and Technology, Huazhong University of Science and Technology, Wuhan, China*

[3] *School of Mathematics, University of Bristol, Bristol, UK*

[4] *Faculty of Life and Environmental Sciences, University of Tsukuba, Ibaraki , Japan*

[*] Address correspondence to: rachel.bennett@bristol.ac.uk, utada.andrew.gm@u.tsukuba.ac.jp, zhiliu@hust.edu.cn, or kunzhao@tju.edu.cn.

[#] These authors contributed equally.

This file includes:

Other supplementary materials for this manuscript include the following:

Movies S1 to S10

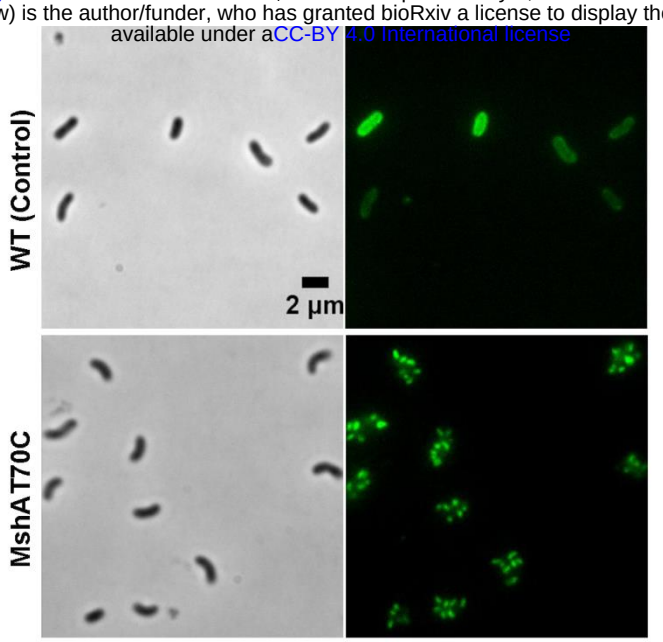

Figure 1-Figure supplement 1. Labeling of *V. cholerae* MSHA pilus protein MshA with AF488-mal.

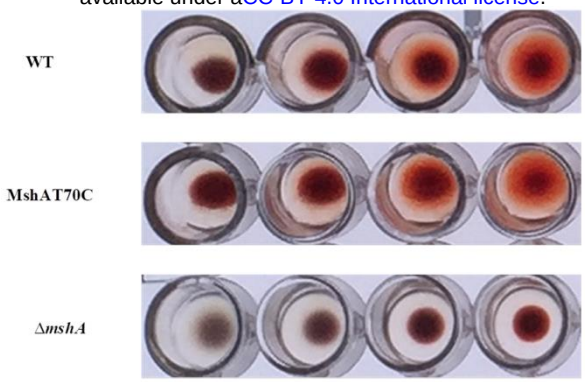

Figure 1-Figure supplement 2. Hemagglutination assays. MshAT70C point mutation does not affect MSHA pilus function. *V. cholerae* strains were grown in LB medium and assayed for MSHA production by hemagglutination. Two-fold dilutions of mid-log cultures of bacteria (left to right) were assayed for their ability to agglutinate sheep erythrocytes. Assay was repeated three times, and representative results are showed.

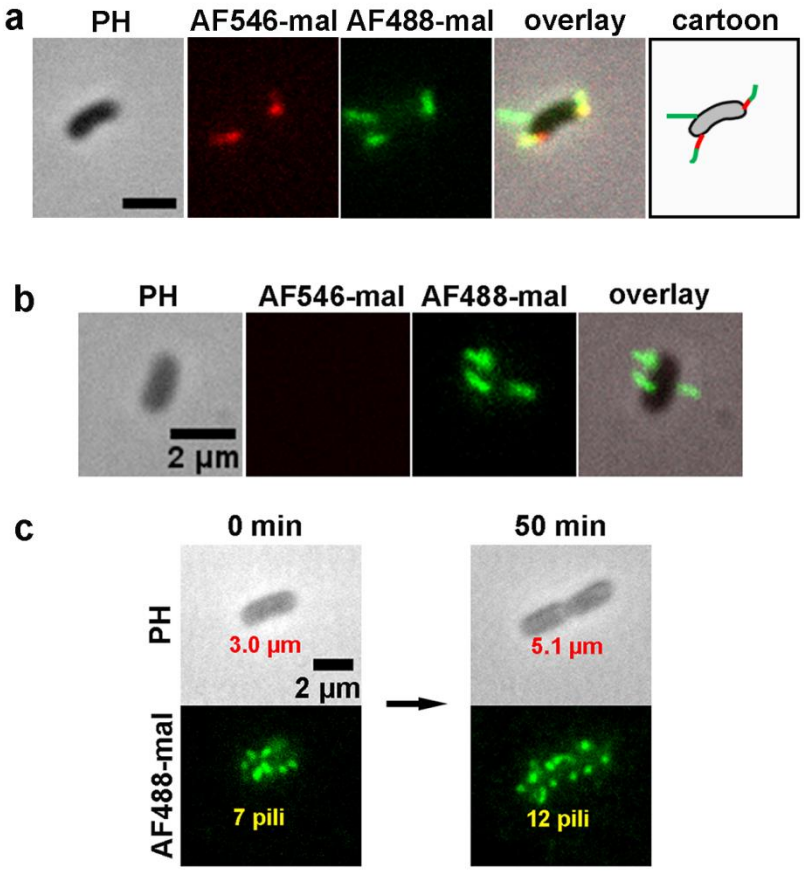

Figure 1-Figure supplement 3. MSHA pili labeling during cell growth. To evaluate changes to the MSHA pilus during cell growth, the MSHA pili were labelled with two different colored dyes, AF546-mal (red) and AF488-mal (green), at 0 min and 40 min, respectively. (a) Representative double-color labeling image of MshAT70C cell, showing the new separate pilus (top left in green) and the secondary segments (lower left, green) at the end of the primary segments (lower left, red). Scale bar, 2 μm. (b) Representative double-color labeling image for a newly dividing cell, which is only labelled with AF488-mal. (c) In situ observation of MSHA pili growth stained at 0 and 50 min with AF488-mal. The results show that during a period of 50 min, the length of the cell changes from 3.0 μm to 5.1 μm, while the number of pili increases from 7 to 12.

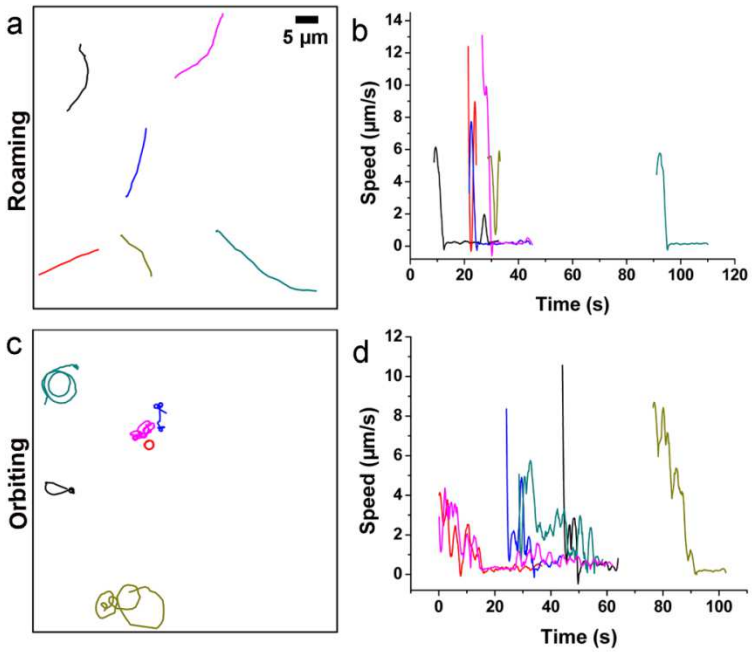

Figure 2-Figure supplement 1. Quantitative analysis of roaming and orbiting by MSHA labelled MshAT70C in 2% LB with 1% MC. (a) Trajectories and (b) speed of typical roaming cells; (c) Trajectories and (d) speed of typical orbiting cells.

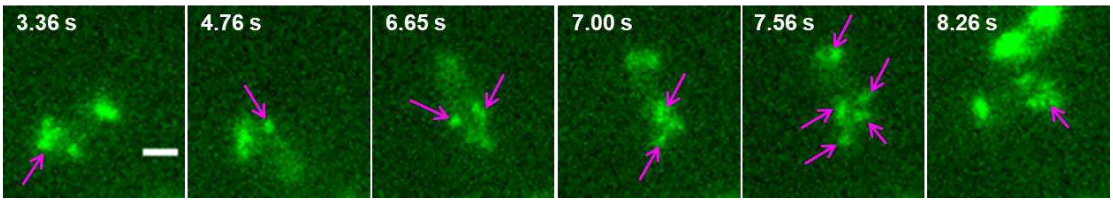

Figure 2-Figure supplement 2. Switch of temporary attached pili. When transient pauses happened, the attached pilus could be switched from one to another or more. The arrows show the apparent pili attached with surface. Scale bar, 1 μm.

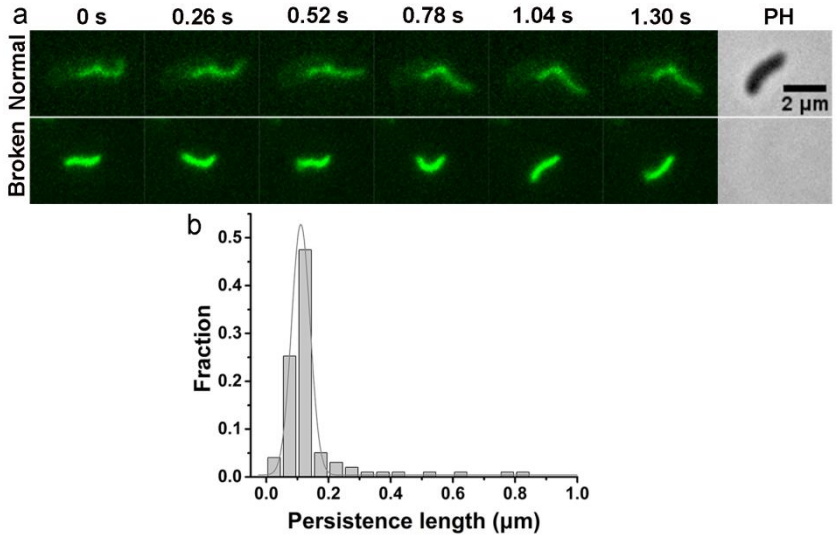

Figure 3-Figure supplement 1. Motion of the broken MSHA pilus. (a) The behavior of normal and broken MSHA pilus. Note that in the phase contrast (PH) image, there is no cell for the broken pili observed in fluorescent images; (b) The persistence lengths of a broken pilus.

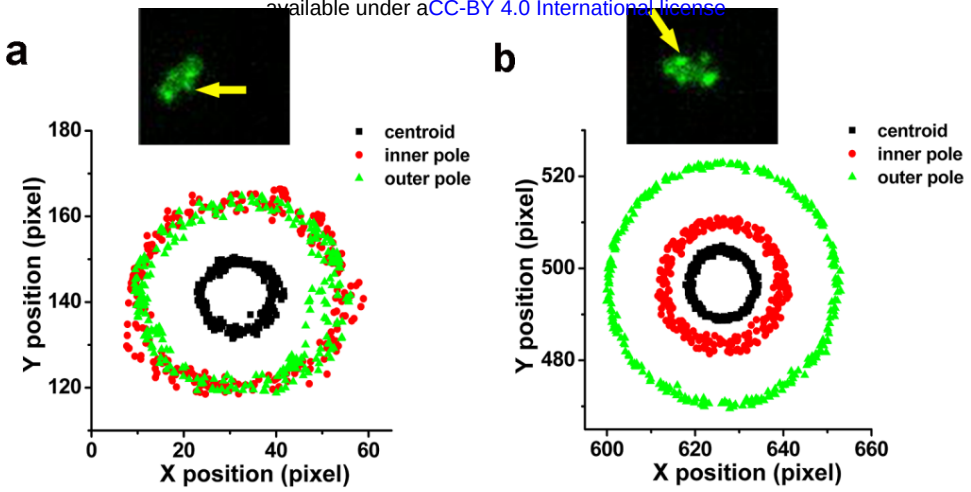

Figure 4-Figure supplement 1. Examples show positions of two poles and centroid of tethered motility. The contributing MSHA pili were indicated by yellow arrows. (a) ~1/2 position; (b) 1/3 or 2/3 position.

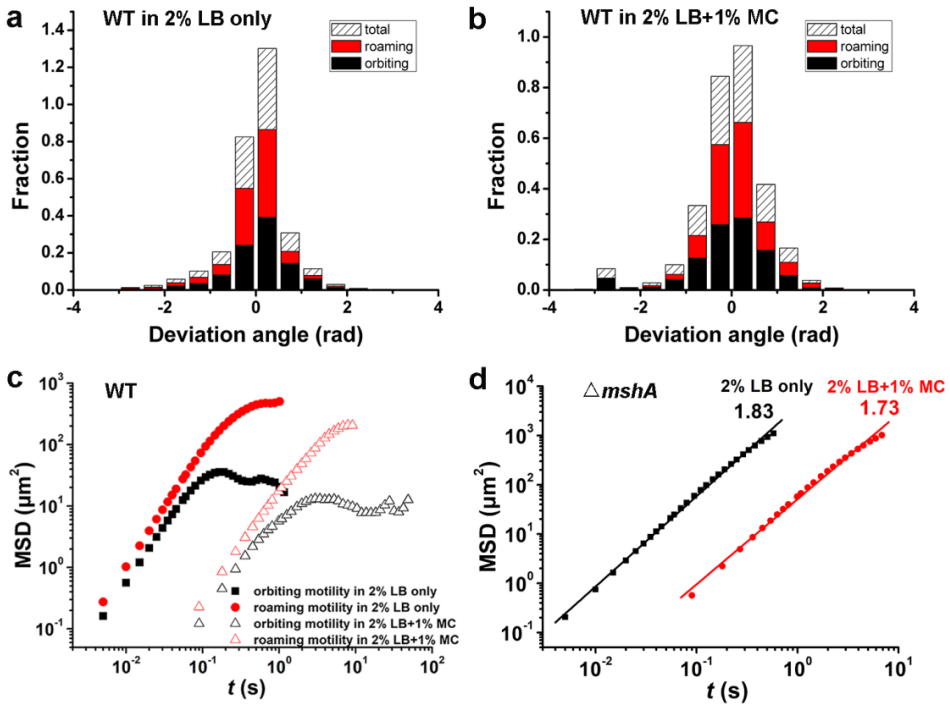

Figure 5-Figure supplement 1. Motility characterization of WT and △*mshA* cells in 2% LB only and in 2% LB with 1% MC. (a) Histograms of deviation angle for WT in 2% LB only. (b) Histograms of deviation angle for WT in 2% LB+1% MC viscous solution. Black represents orbiting motility and red represents roaming motility. (c-d) Mean square displacements (MSDs) of WT (c), △*mshA* (d) in 2% LB only and 2% LB+1% MC viscous solution.

Legends to Supplemental Movies

Movie S1. Time-lapse fluorescence imaging showing a typical roaming cell (indicated by the arrowhead) with labeled MSHA pili in 2% LB+1% MC viscous medium. This movie was shown every 390 ms for 98 s and displayed at 20 frames per second (fps).

Movie S2. Time-lapse fluorescence imaging showing a typical orbiting cell with labeled MSHA pili in 2% LB+1% MC viscous medium. This movie was recorded every 130 ms for 15 s and displayed at 10 fps.

Movie S3. Time-lapse fluorescence imaging showing switch of pili. When transient pauses happened, the attached pilus could be switched from one to another or more. See also Figure S4. This movie was recorded every 70 ms for 10 s and displayed at 5 fps.

Movie S4. Time-lapse fluorescence imaging showing linear motion bent into circular motion that is centered around the attachment point between MSHA pili and the surface, which can act as an anchor point. This movie was recorded every 130 ms for 8 s and displayed at 10 fps.

Movie S5. Time-lapse fluorescence imaging showing dynamic movements of a MshAT70CFlaAA106CS107C cell with labeled flagellum and MSHA pili in 2% LB+1% MC viscous medium. This movie was recorded every 130 ms for 13 s and displayed at 10 fps.

Movie S6. Time-lapse fluorescence imaging showing five MSHA pili of a WT cell stuck to the surface and kept still or fluctuated frequently. This movie was

recorded every 460 ms for 25 s and displayed at 10 fps.

Movie S7. Time-lapse fluorescence imaging showing a broken pilus exfoliated from normal cell exhibiting thermal fluctuations in shape over time. This pilus was attached to the substratum at its right end. This movie was recorded every 130 ms for 29 s and displayed at 10 fps.

Movie S8. Time-lapse fluorescence imaging showing a typical tethered cell performing a circular motion around a fixed point with the direction of motion switched from CCW to CW. See also Figure 4c. This movie was recorded every 130 ms for 6 s and displayed at 5 fps.

Movie S9. Time-lapse fluorescence imaging showing different adhesion points of a pilus. When the tip of the pilus was free (~3.5 s), the upper part of the pilus was still capable of keeping the cell adhered. This movie was recorded every 130 ms for 13 s and displayed at 10 fps.

Movie S10. Time-lapse fluorescence imaging showing the motion evolution of flagellum from rotating to stopping eventually. This movie was recorded every 130 ms for 10 s and displayed at 10 fps.

124 **Table S1. Plasmids, and primers used in this study.**

Plasmids	**Description**	**Source or reference**
pWM91	Suicide vector	(*Metcalf et al., 1996*)
pML3	pWM-FlaAA106C	This study
pML4	pWM-FlaAS107C	This study
pML5	pWM-FlaAA106CS107C	This study
Primer Name	**Primer Sequence (5'→ 3')**	**Description**
VC0409-F1	CTTGTATGGCGCACTCAACG	*mshA* knockout
VC0409-R1-3S	CAGCGCTAATTCAGTTTAAGCGGCCATAGCTACGCAGCATTACTGCAAGG	*mshA* knockout
VC0409-F2-3S	GCTATGGCCGCTTAAACTGAATTAGCGCTGCGTTATACAGCTGCAACCTC	*mshA* knockout
VC0409-R2	CAAGCATAGCCTTGCTGTTC	*mshA* knockout
VC0409-Mut-T70C-R1	GTCTAAACATTCAATGCCTTTAATTGCAGCTCGTCC	MshAT70C construction
VC0409-Mut-T70C-F2	GGCATTGAATGTTTAGACTACACAGCATATAC	MshAT70C construction
VC0409-Mut-Seq-F1	GGCGAAGAAAGCCAGTATTG	MshAT70C detection

		MshAT70C
VC0409-Mut-Seq-R1	CCTGCGGAGAAACTTGAATG	detection
VC2188-F1	CCATGAGACGGTTCGTTTAC	*flaA* knockout
	CAGCGCTAATTCAGTTTAAGCGGCCATAGCGATAACGTTG	
VC2188-R1-3S	TGCGGTCATC	*flaA* knockout
	GCTATGGCCGCTTAAACTGAATTAGCGCTGCAGTAGTTCA	
VC2188-F2-3S	CGGTACCTTC	*flaA* knockout
VC2188-R2	CCAAAGATGCCGGTAAATGG	*flaA* knockout
		FlaA
		mutations
VC2188-Mut-F1	CACACTTTGGTTTCCGGTAC	construction
		FlaA
		mutations
VC2188-Mut-R2	TCCGCACCATTATTGAGAGC	construction
		FlaAA106C
VC2188-Mut-A106C-R1	TGACGCTCTGAACATGAGTTGGTACCGTTCGCCGA	construction
		FlaAA106C
VC2188-Mut-A106C-F2	AACGGTACCAACTCATGTTCAGAGCGTCAGGCTC	construction
		FlaAS107C
VC2188-Mut-S107C-R1	TGACGCTCACACGCTGAGTTGGTACCGTTCGCCGAT	construction
		FlaAS107C
VC2188-Mut-S107C-F2	AACGGTACCAACTCAGCGTGTGAGCGTCAGGCTCTG	construction

		FlaAA106CS1
VC2188-Mut-A106C-S1		07C
07C-R1	TGACGCTCACAACATGAGTTGGTACCGTTCGCCGAT	construction
		FlaAA106CS1
VC2188-Mut-A106C-S1		07C
07C-F2	AACGGTACCAACTCATGTTGTGAGCGTCAGGCTCTG	construction
		FlaAE332C
VC2188-Mut-E332C-R1	CGACGCACACACGTTCTCCTGAATATTCGACAG	construction
		FlaAE332C
VC2188-Mut-E332C-F2	ATATTCAGGAGAACGTGTGTGCGTCGAAAAGTC	construction
		FlaAG23C
VC2188-Mut-G23C-R1	GTTAAGCTCACACGTCGCCTTGGTCAGATAACGTTGTG	construction
		FlaAG23C
VC2188-Mut-G23C-F2	TATCTGACCAAGGCGACGTGTGAGCTTAACACCTCCA	construction
		FlaAN26C
VC2188-Mut-N26C-R1	TCCATGGAGGTACAAAGCTCTCCCGTCGCCTTGGT	construction
		FlaAN26C
VC2188-Mut-N26C-F2	ACGGGAGAGCTTTGTACCTCCATGGAACGCCTCTCA	construction
		FlaAN83C
VC2188-Mut-N83C-R1	GTCGATTCACACATCGCACCTTCTGCGGTTTGAG	construction
		FlaAN83C
VC2188-Mut-N83C-F2	AGAAGGTGCGATGTGTGAATCGACCAGCATTTTGCAGC	construction

		FlaAS325C
VC2188-Mut-S325C-R1	GTTCTCCTGAATATTACACAGGTTACTGATGCTGTGAC	construction
	ATCAGTAACCTGTGTAATATTCAGGAGAACGTGGAAGCG	FlaAS325C
VC2188-Mut-S325C-F2	TC	construction
		FlaAS87C
VC2188-Mut-S87C-R1	CGCTGCAAAATACAGGTCGATTCATTCATCGCACCT	construction
		FlaAS87C
VC2188-Mut-S87C-F2	GAATCGACCTGTATTTTGCAGCGTATGCGTGACCTC	construction
		FlaAS376C
VC2188-Mut-S376C-R1	GTGAACTACTGCAATAAACAGATTGCAGAGTTTGGC	construction
		FlaAS376C
VC2188-Mut-S376C-F2	TGCAATCTGTTTATTGCAGTAGTTCACGGTACCTTC	construction
		FlaAV117C
VC2188-Mut-V117C-R1	ATCTTGCAGTGCACACGACTCTTCATTCAGAGCCTG	construction
		FlaAV117C
VC2188-Mut-V117C-F2	GAAGAGTCGTGTGCACTGCAAGATGAACTGAACCGTA	construction
		FlaA
		mutations
VC2188-Mut-Seq-F1	TGAGCTTGCGAACTCGATAG	detection
		FlaA
		mutations
VC2188-Mut-Seq-R1	CGTTCTTCAGCGGATGATAG	detection

Supplementary references

Metcalf WW, Jiang W, Daniels LL, Kim SK, Haldimann A, Wanner BL. 1996. Conditionally replicative and conjugative plasmids carrying lacZ alpha for cloning, mutagenesis, and allele replacement in bacteria. *Plasmid* **35**: 1-13. DOI: 10.1006/plas.1996.0001, PMID: 8693022

Supplementary information for

Crash landing of *Vibrio cholerae* by MSHA pili-assisted braking and anchoring in a viscous environment

Wenchao Zhang[1,#], Mei Luo[2,#], Chunying Feng[1], Rachel R. Bennett[3,*], Andrew S. Utada[4,*], Zhi Liu[2,*], Kun Zhao[1,*]

[1] *Frontier Science Center for Synthetic Biology and Key Laboratory of Systems Bioengineering (Ministry of Education), School of Chemical Engineering and Technology, Tianjin University, Tianjin, P.R. China*

[2] *Department of Biotechnology, College of Life Science and Technology, Huazhong University of Science and Technology, Wuhan, China*

[3] *School of Mathematics, University of Bristol, Bristol, UK*

[4] *Faculty of Life and Environmental Sciences, University of Tsukuba, Ibaraki , Japan*

[*] Address correspondence to: rachel.bennett@bristol.ac.uk, utada.andrew.gm@u.tsukuba.ac.jp, zhiliu@hust.edu.cn, or kunzhao@tju.edu.cn.

[#] These authors contributed equally.

This file includes:

Other supplementary materials for this manuscript include the following:

Movies S1 to S10

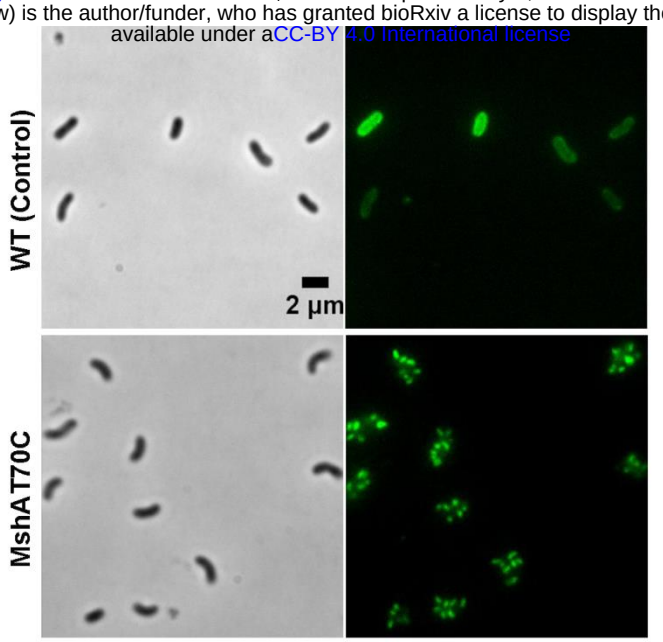

Figure 1-Figure supplement 1. Labeling of *V. cholerae* MSHA pilus protein MshA with AF488-mal.

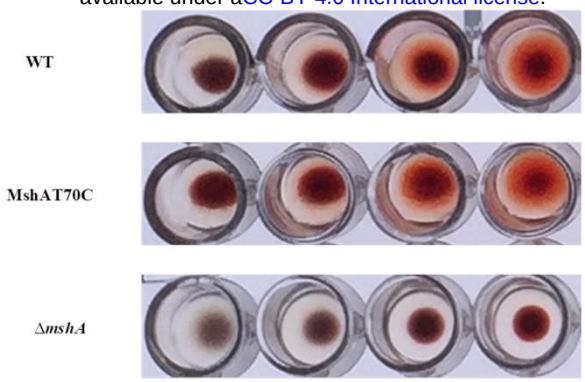

Figure 1-Figure supplement 2. Hemagglutination assays. MshAT70C point mutation does not affect MSHA pilus function. *V. cholerae* strains were grown in LB medium and assayed for MSHA production by hemagglutination. Two-fold dilutions of mid-log cultures of bacteria (left to right) were assayed for their ability to agglutinate sheep erythrocytes. Assay was repeated three times, and representative results are showed.

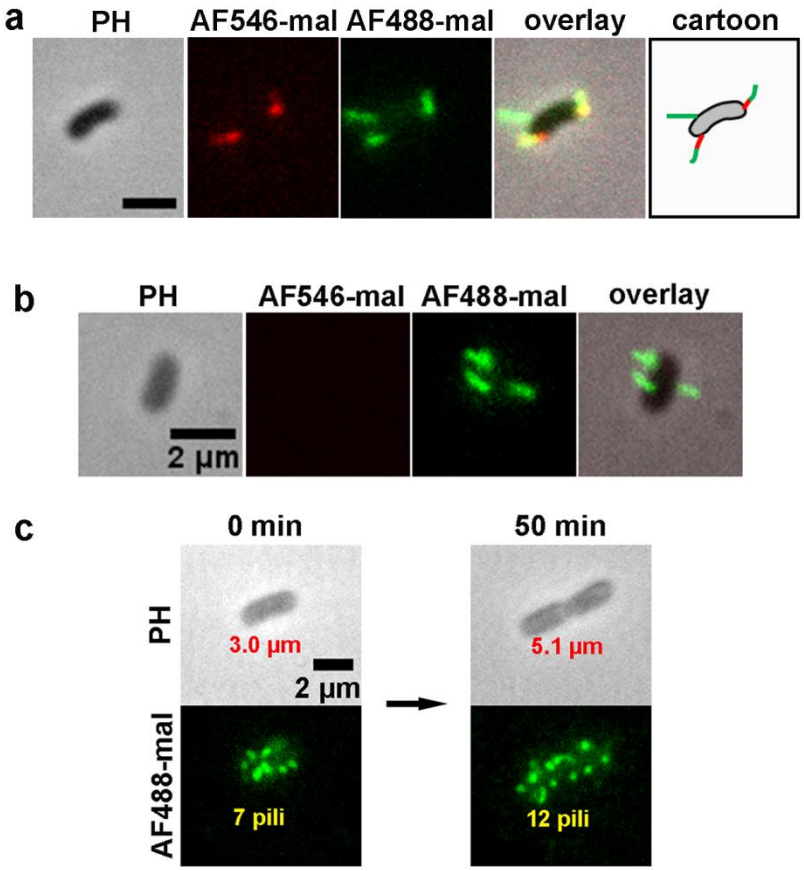

Figure 1-Figure supplement 3. MSHA pili labeling during cell growth. To evaluate changes to the MSHA pilus during cell growth, the MSHA pili were labelled with two different colored dyes, AF546-mal (red) and AF488-mal (green), at 0 min and 40 min, respectively. (a) Representative double-color labeling image of MshAT70C cell, showing the new separate pilus (top left in green) and the secondary segments (lower left, green) at the end of the primary segments (lower left, red). Scale bar, 2 μm. (b) Representative double-color labeling image for a newly dividing cell, which is only labelled with AF488-mal. (c) In situ observation of MSHA pili growth stained at 0 and 50 min with AF488-mal. The results show that during a period of 50 min, the length of the cell changes from 3.0 μm to 5.1 μm, while the number of pili increases from 7 to 12.

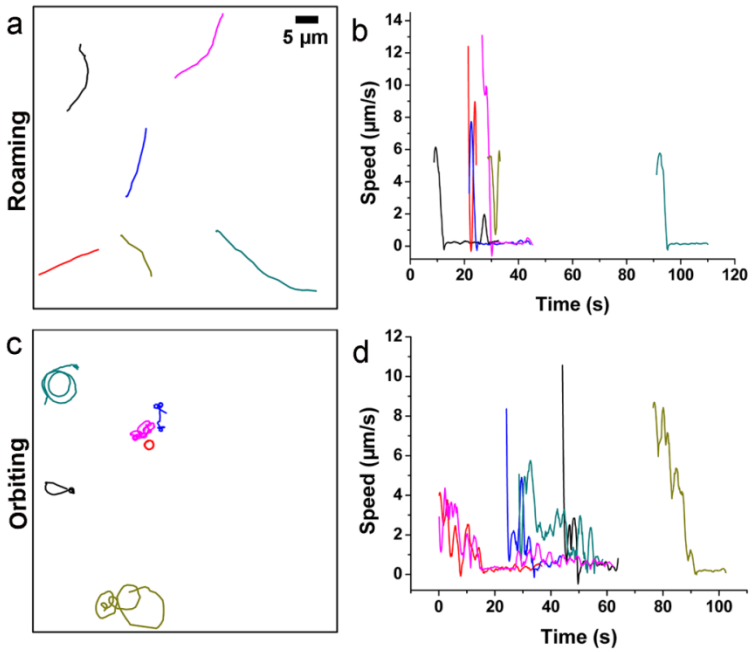

Figure 2-Figure supplement 1. Quantitative analysis of roaming and orbiting by MSHA labelled MshAT70C in 2% LB with 1% MC. (a) Trajectories and (b) speed of typical roaming cells; (c) Trajectories and (d) speed of typical orbiting cells.

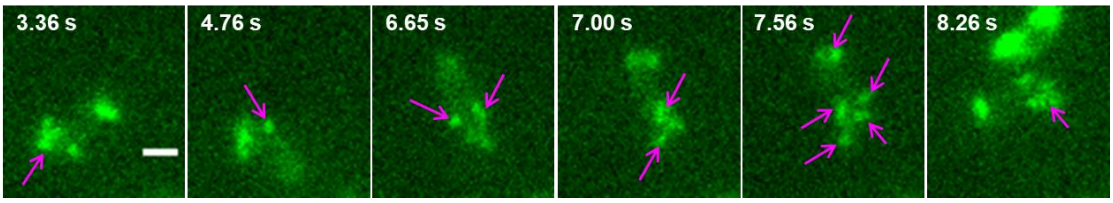

Figure 2-Figure supplement 2. Switch of temporary attached pili. When transient pauses happened, the attached pilus could be switched from one to another or more. The arrows show the apparent pili attached with surface. Scale bar, 1 μm.

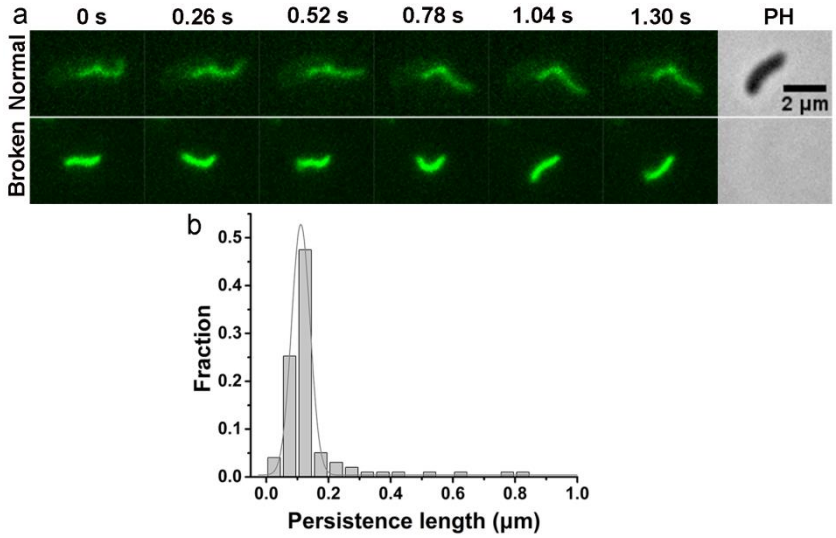

Figure 3-Figure supplement 1. Motion of the broken MSHA pilus. (a) The behavior of normal and broken MSHA pilus. Note that in the phase contrast (PH) image, there is no cell for the broken pili observed in fluorescent images; (b) The persistence lengths of a broken pilus.

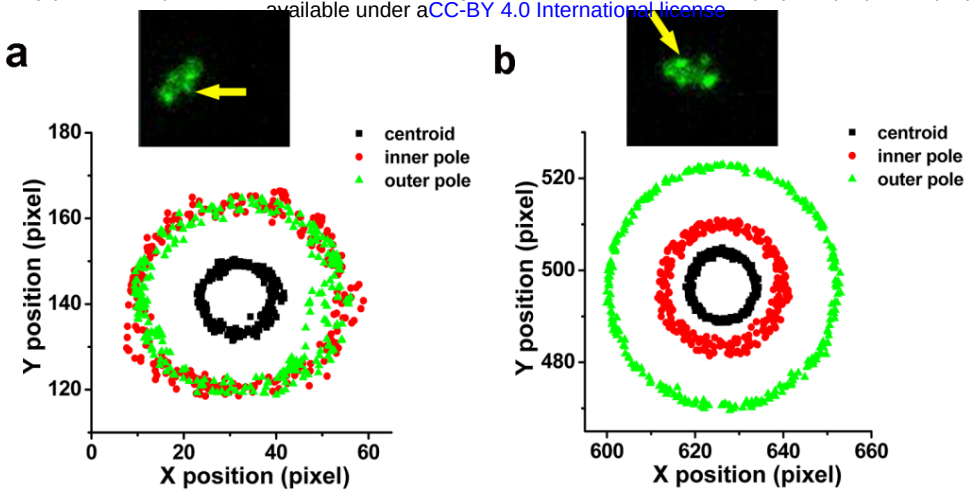

Figure 4-Figure supplement 1. Examples show positions of two poles and centroid of tethered motility. The contributing MSHA pili were indicated by yellow arrows. (a) ~1/2 position; (b) 1/3 or 2/3 position.

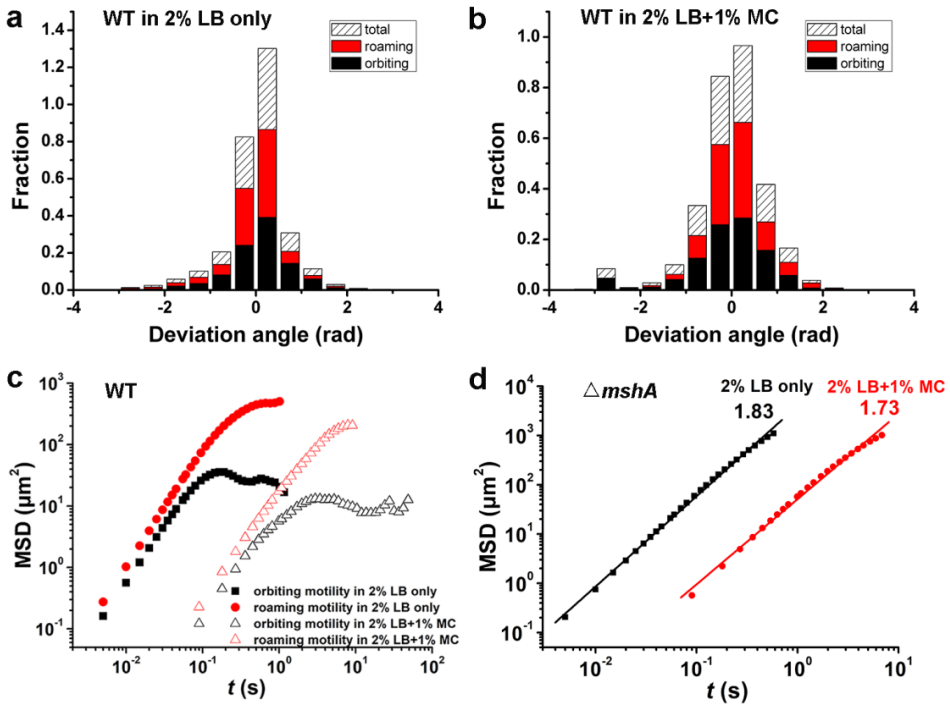

Figure 5-Figure supplement 1. Motility characterization of WT and △*mshA* cells in 2% LB only and in 2% LB with 1% MC. (a) Histograms of deviation angle for WT in 2% LB only. (b) Histograms of deviation angle for WT in 2% LB+1% MC viscous solution. Black represents orbiting motility and red represents roaming motility. (c-d) Mean square displacements (MSDs) of WT (c), △*mshA* (d) in 2% LB only and 2% LB+1% MC viscous solution.

Legends to Supplemental Movies

Movie S1. Time-lapse fluorescence imaging showing a typical roaming cell (indicated by the arrowhead) with labeled MSHA pili in 2% LB+1% MC viscous medium. This movie was shown every 390 ms for 98 s and displayed at 20 frames per second (fps).

Movie S2. Time-lapse fluorescence imaging showing a typical orbiting cell with labeled MSHA pili in 2% LB+1% MC viscous medium. This movie was recorded every 130 ms for 15 s and displayed at 10 fps.

Movie S3. Time-lapse fluorescence imaging showing switch of pili. When transient pauses happened, the attached pilus could be switched from one to another or more. See also Figure S4. This movie was recorded every 70 ms for 10 s and displayed at 5 fps.

Movie S4. Time-lapse fluorescence imaging showing linear motion bent into circular motion that is centered around the attachment point between MSHA pili and the surface, which can act as an anchor point. This movie was recorded every 130 ms for 8 s and displayed at 10 fps.

Movie S5. Time-lapse fluorescence imaging showing dynamic movements of a MshAT70CFlaAA106CS107C cell with labeled flagellum and MSHA pili in 2% LB+1% MC viscous medium. This movie was recorded every 130 ms for 13 s and displayed at 10 fps.

Movie S6. Time-lapse fluorescence imaging showing five MSHA pili of a WT cell stuck to the surface and kept still or fluctuated frequently. This movie was

recorded every 460 ms for 25 s and displayed at 10 fps.

Movie S7. Time-lapse fluorescence imaging showing a broken pilus exfoliated from normal cell exhibiting thermal fluctuations in shape over time. This pilus was attached to the substratum at its right end. This movie was recorded every 130 ms for 29 s and displayed at 10 fps.

Movie S8. Time-lapse fluorescence imaging showing a typical tethered cell performing a circular motion around a fixed point with the direction of motion switched from CCW to CW. See also Figure 4c. This movie was recorded every 130 ms for 6 s and displayed at 5 fps.

Movie S9. Time-lapse fluorescence imaging showing different adhesion points of a pilus. When the tip of the pilus was free (~3.5 s), the upper part of the pilus was still capable of keeping the cell adhered. This movie was recorded every 130 ms for 13 s and displayed at 10 fps.

Movie S10. Time-lapse fluorescence imaging showing the motion evolution of flagellum from rotating to stopping eventually. This movie was recorded every 130 ms for 10 s and displayed at 10 fps.

124 **Table S1. Plasmids, and primers used in this study.**

Plasmids	**Description**	**Source or reference**
pWM91	Suicide vector	(*Metcalf et al., 1996*)
pML3	pWM-FlaAA106C	This study
pML4	pWM-FlaAS107C	This study
pML5	pWM-FlaAA106CS107C	This study
Primer Name	**Primer Sequence (5'→ 3')**	**Description**
VC0409-F1	CTTGTATGGCGCACTCAACG	*mshA* knockout
VC0409-R1-3S	CAGCGCTAATTCAGTTTAAGCGGCCATAGCTACGCAGCATTACTGCAAGG	*mshA* knockout
VC0409-F2-3S	GCTATGGCCGCTTAAACTGAATTAGCGCTGCGTTATACAGCTGCAACCTC	*mshA* knockout
VC0409-R2	CAAGCATAGCCTTGCTGTTC	*mshA* knockout
VC0409-Mut-T70C-R1	GTCTAAACATTCAATGCCTTTAATTGCAGCTCGTCC	MshAT70C construction
VC0409-Mut-T70C-F2	GGCATTGAATGTTTAGACTACACAGCATATAC	MshAT70C construction
VC0409-Mut-Seq-F1	GGCGAAGAAAGCCAGTATTG	MshAT70C detection

		MshAT70C
VC0409-Mut-Seq-R1	CCTGCGGAGAAACTTGAATG	detection
VC2188-F1	CCATGAGACGGTTCGTTTAC	*flaA* knockout
	CAGCGCTAATTCAGTTTAAGCGGCCATAGCGATAACGTTG	
VC2188-R1-3S	TGCGGTCATC	*flaA* knockout
	GCTATGGCCGCTTAAACTGAATTAGCGCTGCAGTAGTTCA	
VC2188-F2-3S	CGGTACCTTC	*flaA* knockout
VC2188-R2	CCAAAGATGCCGGTAAATGG	*flaA* knockout
		FlaA
		mutations
VC2188-Mut-F1	CACACTTTGGTTTCCGGTAC	construction
		FlaA
		mutations
VC2188-Mut-R2	TCCGCACCATTATTGAGAGC	construction
		FlaAA106C
VC2188-Mut-A106C-R1	TGACGCTCTGAACATGAGTTGGTACCGTTCGCCGA	construction
		FlaAA106C
VC2188-Mut-A106C-F2	AACGGTACCAACTCATGTTCAGAGCGTCAGGCTC	construction
		FlaAS107C
VC2188-Mut-S107C-R1	TGACGCTCACACGCTGAGTTGGTACCGTTCGCCGAT	construction
		FlaAS107C
VC2188-Mut-S107C-F2	AACGGTACCAACTCAGCGTGTGAGCGTCAGGCTCTG	construction

		FlaAA106CS1
VC2188-Mut-A106C-S1		07C
07C-R1	TGACGCTCACAACATGAGTTGGTACCGTTCGCCGAT	construction
		FlaAA106CS1
VC2188-Mut-A106C-S1		07C
07C-F2	AACGGTACCAACTCATGTTGTGAGCGTCAGGCTCTG	construction
		FlaAE332C
VC2188-Mut-E332C-R1	CGACGCACACACGTTCTCCTGAATATTCGACAG	construction
		FlaAE332C
VC2188-Mut-E332C-F2	ATATTCAGGAGAACGTGTGTGCGTCGAAAAGTC	construction
		FlaAG23C
VC2188-Mut-G23C-R1	GTTAAGCTCACACGTCGCCTTGGTCAGATAACGTTGTG	construction
		FlaAG23C
VC2188-Mut-G23C-F2	TATCTGACCAAGGCGACGTGTGAGCTTAACACCTCCA	construction
		FlaAN26C
VC2188-Mut-N26C-R1	TCCATGGAGGTACAAAGCTCTCCCGTCGCCTTGGT	construction
		FlaAN26C
VC2188-Mut-N26C-F2	ACGGGAGAGCTTTGTACCTCCATGGAACGCCTCTCA	construction
		FlaAN83C
VC2188-Mut-N83C-R1	GTCGATTCACACATCGCACCTTCTGCGGTTTGAG	construction
		FlaAN83C
VC2188-Mut-N83C-F2	AGAAGGTGCGATGTGTGAATCGACCAGCATTTTGCAGC	construction

		FlaAS325C
VC2188-Mut-S325C-R1	GTTCTCCTGAATATTACACAGGTTACTGATGCTGTGAC	construction
	ATCAGTAACCTGTGTAATATTCAGGAGAACGTGGAAGCG	FlaAS325C
VC2188-Mut-S325C-F2	TC	construction
		FlaAS87C
VC2188-Mut-S87C-R1	CGCTGCAAAATACAGGTCGATTCATTCATCGCACCT	construction
		FlaAS87C
VC2188-Mut-S87C-F2	GAATCGACCTGTATTTTGCAGCGTATGCGTGACCTC	construction
		FlaAS376C
VC2188-Mut-S376C-R1	GTGAACTACTGCAATAAACAGATTGCAGAGTTTGGC	construction
		FlaAS376C
VC2188-Mut-S376C-F2	TGCAATCTGTTTATTGCAGTAGTTCACGGTACCTTC	construction
		FlaAV117C
VC2188-Mut-V117C-R1	ATCTTGCAGTGCACACGACTCTTCATTCAGAGCCTG	construction
		FlaAV117C
VC2188-Mut-V117C-F2	GAAGAGTCGTGTGCACTGCAAGATGAACTGAACCGTA	construction
		FlaA
		mutations
VC2188-Mut-Seq-F1	TGAGCTTGCGAACTCGATAG	detection
		FlaA
		mutations
VC2188-Mut-Seq-R1	CGTTCTTCAGCGGATGATAG	detection

Supplementary references

Metcalf WW, Jiang W, Daniels LL, Kim SK, Haldimann A, Wanner BL. 1996. Conditionally replicative and conjugative plasmids carrying lacZ alpha for cloning, mutagenesis, and allele replacement in bacteria. *Plasmid* **35**: 1-13. DOI: 10.1006/plas.1996.0001, PMID: 8693022